Joule

CellPress

Article

Liquid Thermo-Responsive Smart Window Derived from Hydrogel

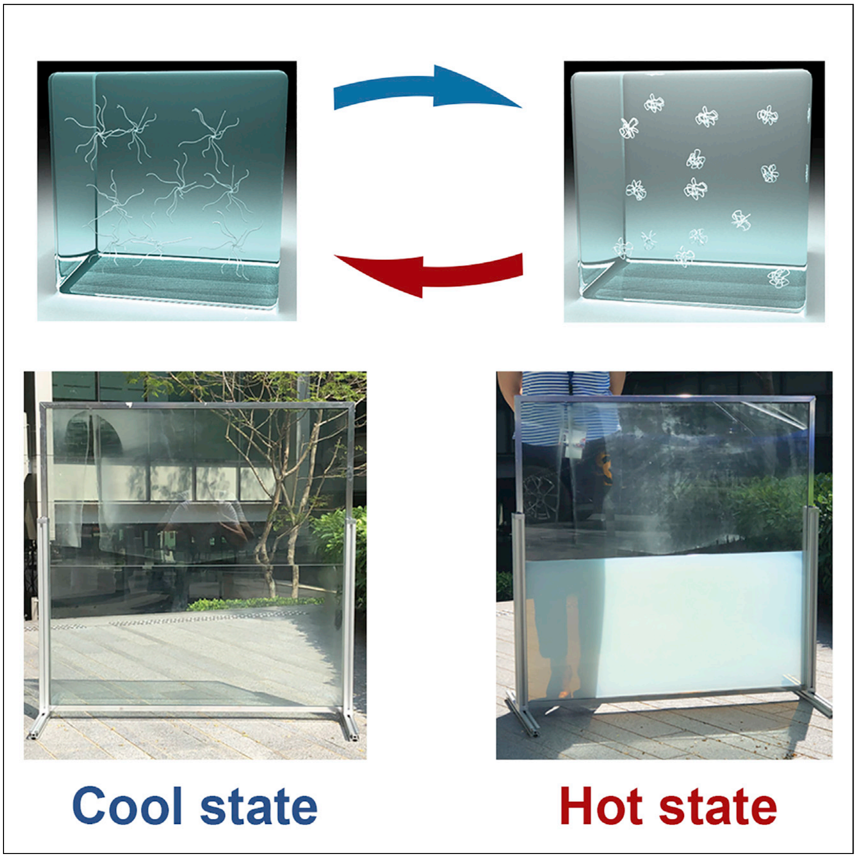

Buildings account for 40% of global energy consumption, while windows are the least energy-efficient part of buildings. Conventional smart windows only regulate solar transmission. For the first time, a smart thermochromic window with high thermal energy storage was developed to cut off building energy consumption as demonstrated by experiments and simulations. The first liquid encapsulated glass panel gives unique advantages of high uniformity, easy fabrication, shape independence, scalability, and soundproofing.

Yang Zhou, Shancheng Wang, Jinqing Peng, Yutong Tan, Chuanchang Li, Freddy Yin Chiang Boey, Yi Long

longyi@ntu.edu.sg

HIGHLIGHTS

A liquid-filled smart window with excellent thermochromic performance

Large thermal energy storage capability to shift the electricity load peak

Combining solar regulation and heat storage to cut off building energy consumption

Better soundproof function than double-glazed glass with good scalability

Zhou et al., Joule 4, 1–17
November 18, 2020
https://doi.org/10.1016/j.joule.2020.09.001

Please cite this article in press as: Zhou et al., Liquid Thermo-Responsive Smart Window Derived from Hydrogel, Joule (2020), https://doi.org/10.1016/j.joule.2020.09.001

Joule

CellPress

Article

Liquid Thermo-Responsive Smart Window Derived from Hydrogel

Yang Zhou,[1,2,7] Shancheng Wang,[1,2,7] Jinqing Peng,[3] Yutong Tan,[3] Chuanchang Li,[4] Freddy Yin Chiang Boey,[5] and Yi Long[1,2,6,8,*]

SUMMARY

Buildings account for 40% of global energy consumption, while windows are the least energy-efficient part of buildings. Conventional smart windows only regulate solar transmission. For the first time, we developed high thermal energy storage thermo-responsive smart window (HTEST smart window) by trapping the hydrogel-derived liquid within glasses. The excellent thermo-responsive optical property (90% of luminous transmittance and 68.1% solar modulation) together with outstanding specific heat capacity of liquid gives the HTEST smart window excellent energy conservation performance. Simulations suggested that HTEST window can cut off 44.6% heating, ventilation, and air-conditioning (HVAC) energy consumption compared with the normal glass in Singapore. In outdoor demonstrations, the HTEST smart window showed promising energy-saving performance in summer daytime. Compared with conventional energy-saving glasses, which need expensive equipment, the thermo-responsive liquid-trapped structure offers a disruptive strategy of easy fabrication, good uniformity, and scalability, together with soundproof functionality that opens an avenue for energy-saving buildings and greenhouses.

INTRODUCTION

In 2018, the Intergovernmental Panel on Climate Change (IPCC) reduced the global warming allowance from 2°C to 1.5°C to alarm the great urgency of climate change, which emphasized the significance of energy conservation and carbon emission reduction.[1] The building sector consumes approximately 40% of the total energy, while heating, ventilation, and air-conditioning (HVAC) consume half of the energy in buildings.[2,3] To address this issue, improving building energy efficiency is critical in energy conservation.

Windows are considered as the least energy-efficient part of the building envelope. In hot seasons, most of the window-directed solar energy will be converted into heat and lead to high cooling demand, while in winter, windows are responsible for 30% of energy loss.[4–6] The most studied energy-saving windows are focused on chromogenic technologies, including electrochromic, photochromic, and thermochromic.[7–11] Examples of chromogenic materials includes hydrogels[12] and liquid crystals.[13–15] Among three, thermochromic materials are considered as the most cost-effective, rational stimulus and zero energy input properties.[16–18] However, it is an inevitable challenge to further enhance its energy-saving capability due to the intrinsic limits of conventional thermochromic materials.[19]

Context & Scale

Buildings account for 40% of global energy consumption, while windows are the least energy-efficient part of buildings. Thermochromic window responds to temperature automatically to regulate the solar transmission solely. In this work, a smart window that combines good thermochromic performance and large thermal energy storage capability was introduced. At lower temperature, the window is transparent to let in the solar transmission; when heated, the window blocks sunlight automatically to cut off solar gain. The added function of heat storage further reduces the energy consumption and shift the electricity load peak to lower price period. This first thermo-responsive liquid encapsulated window panel offers a think-out-of-box strategy, giving unique advantage of easy fabrication, good uniformity, scalability, and soundproofing.

Please cite this article in press as: Zhou et al., Liquid Thermo-Responsive Smart Window Derived from Hydrogel, Joule (2020), https://doi.org/10.1016/j.joule.2020.09.001

All the studied smart windows only regulate light transmission. However, the heating and cooling of the house are much more complicated. High thermal energy storage (TES) materials are widely used in walls,[20] floors,[21] and roofs[22] because they can reduce cooling/heating loads and shift energy load to low price periods.[23–27] According to their principle of thermal energy storing, TES materials can be categorized into sensible heat storage material, latent heat material, and chemical heat storage material.[28,29] To ensure a stable and satisfied performance, the TES materials need to have good specific heat capacity. The good specific heat capacity ensures that TES material is able to store large amount of heat, while the relatively high thermal conductivity allows the uniform distribution of the heat stored in the material and improves the heat storage efficiency. Also, TES material needs to meet some physical requirements like high cycle stability, non-corrosiveness, and low system complexity.[30] The majority building materials such as wood, metal, glass, and concrete generally have low TES less than 100 kJ kg^{-1} ranging from 10°C–70°C (Figure 1A; Table S1). Some commercially available high TES materials include paraffin, fatty acid, and inorganic salt, a category of phase change materials (PCMs), are not suitable in glass due to the lack of luminous transparency, which is critical for windows.

Water, due to its outstanding specific heat capacity (4.2 kJ kg^{-1} K^{-1}), has a significantly higher TES capability (~250 kJ kg^{-1}) than the majority of construction materials (Figure 1A; Table S1).[54] Hereby, we developed a revolutionary high energy storage thermo-responsive smart window (HTEST smart window), which leverages high solar energy modulation together with high TES capability intrinsic in water-rich thermo-responsive liquid (TRL), which is derived from usual hydrogel.[55] As showed in Figure 1B, the HTEST window is designed with poly (N-isopropylacrylamide) (PNIPAm) hydrogel particles dispersed in water, which are trapped between two layers of glasses. The conventional thermo-responsive hydrogel is in the gel form and laminated between glasses to regulate the light transmittance solely.[56–58] The newly developed TRL experience a similar hydrophilic to hydrophobic transition at the lower critical solution temperature (LCST) as conventional hydrogel; below the LCST, the water molecules are within the PNIPAm macromolecules, which give high transparency, allowing the high solar transmission to heat the room in winter. Once heated above the LCST, the water molecules will be released from the PNIPAm, and the shrinkage particles will cause scattering of the light (Figure 1C). We would like to highlight that different from the *in situ* synthesis technique used for the production of conventional hydrogel,[55,58] the newly developed TRL is synthesized by dispersing PNIPAm particles into water and form the homogeneous solution, which gives it an advantage of free flowing. Although the current thermo-responsive hydrogel has been intensively investigated,[59–63] none of the work discusses the thermal capacity concept and none of them are free flow. We adopted the new form of the TRL acting as an energy storage layer with the additional functionality of absorbing and storing the energy. The liquid phase gives a unique advantage of easy fabrication (by simply pouring into the double-glazed glass, Figure 1D; Video S1) as well as the high potential of scaling up and uniformity (Figure 1E), which are difficult and costly in the conventional low-E glass as the expensive setup is a must.

The fabricated HTEST smart window showed a high luminous transmittance (T_{lum}) of ~90% and a high solar modulating ability (ΔT_{sol}) of 68.1%. Moreover, the TES of 261 kJ kg^{-1} is achieved in the temperature range of 10°C~70°C due to a higher specific heat capacity (C_p) of TRL than water (252 kJ kg^{-1}). The excellent energy-saving performance was proved by the simulation and actual indoor and outdoor demonstration compared with conventional glasses. The HTEST has the added benefits

[1]School of Materials Science and Engineering, Nanyang Technological University, Singapore 639798, Singapore

[2]Singapore-HUJ Alliance for Research and Enterprise (SHARE), Campus for Research Excellence and Technological Enterprise (CREATE), Singapore 138602, Singapore

[3]College of Civil Engineering, Hunan University, Changsha 410082, China

[4]School of Energy and Power Engineering, Changsha University of Science and Technology, Changsha 410114, China

[5]Biomedical Engineering Department, National University of Singapore, Singapore 117583, Singapore

[6]Sino-Singapore International Joint Research Institute (SSIJRI), Guangzhou 510000, China

[7]These authors contributed equally

[8]Lead Contact

*Correspondence: longyi@ntu.edu.sg

https://doi.org/10.1016/j.joule.2020.09.001

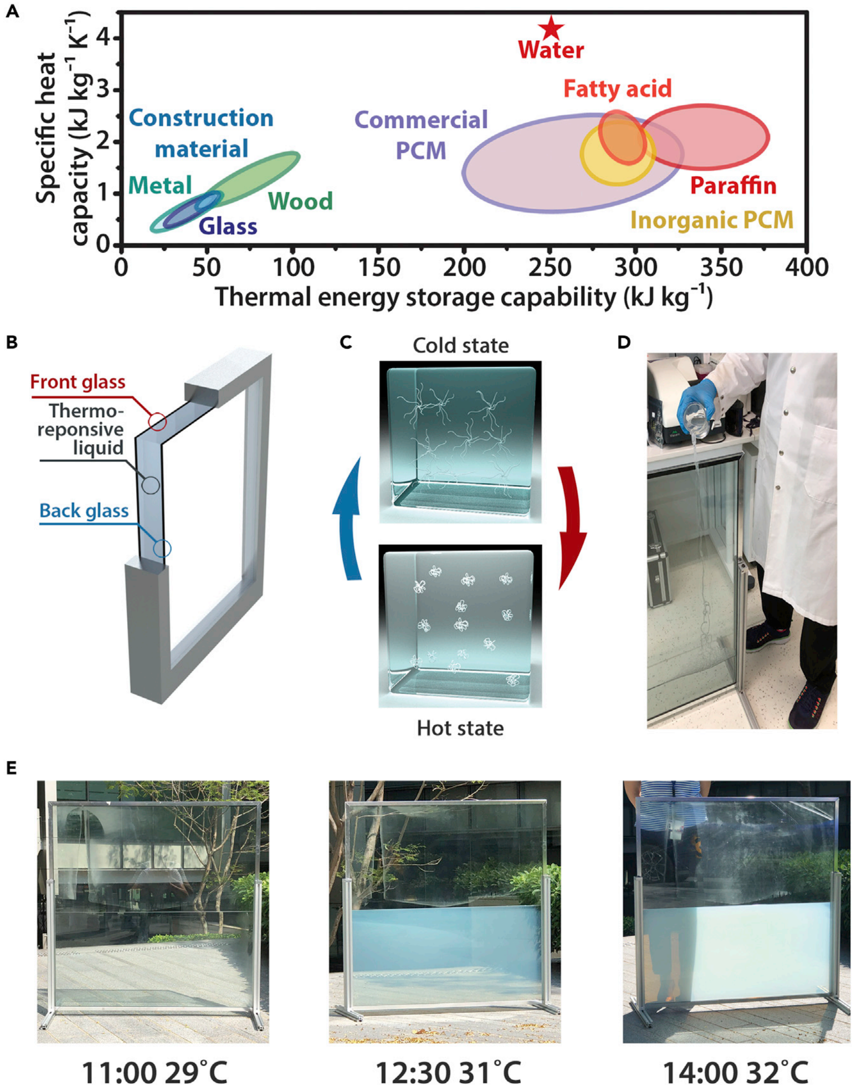

Figure 1. Concept and Photo of HTEST Smart Window

(A) Performance comparison of specific heat capacity and TES ranging from 10°C–70°C for water,[31] paraffin,[23,32–34] fatty acid,[35–39] inorganic PCMs,[40–42] commercial PCMs,[43–47] metal,[48,49] glass,[23,31] construction materials,[48,50] and wood.[51–53]

(B) Structure of the HTEST smart window.

(C) Microstructure scheme for the cooling and heating stage of the liquid.

(D) Filling process of the liquid.

(E) Optical photos for 1-m^2 large-scale window testing at a different time of a day. The TRL is half-filled in the window (0.5 m × 1 m).

of no constraint of window shape and good potential of soundproofing due to the free-flowing liquid.[64] HTEST smart window may revolutionize the window industry with the outstanding energy-saving performance, which has a high potential for commercialization.

RESULTS

Optical and Thermal Properties of the TRL

Figure 2A shows the transmittance spectra of the TRL with thicknesses of 0.1, 1 mm, and 1 cm at 20°C and 60°C, respectively. At room temperature, all the samples show

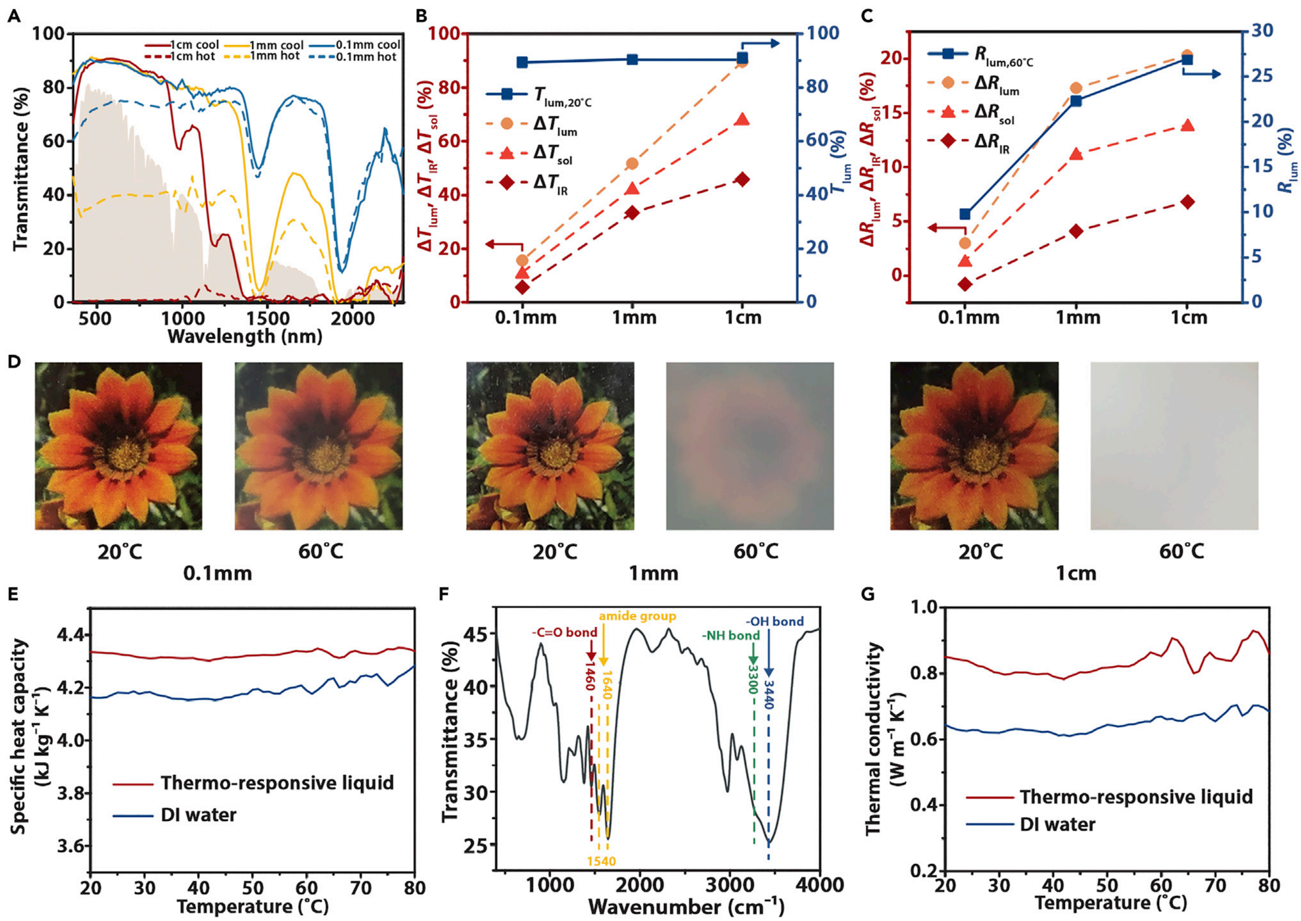

Figure 2. Optical and Thermal Properties of the TRL

(A) Transmittance spectra for 0.1, 1 mm, and 1 cm at 20°C (solid line) and 60°C (dashed line), respectively. The gray shadow in the figure represents the spectrum of sunlight in the visible and NIR range.

(B) The optical performance comparison on the luminous transmittance at 20°C ($T_{lum,20°C}$), luminous transmittance difference (ΔT_{lum}), IR transmittance difference (ΔT_{IR}), and solar modulating ability (ΔT_{sol}) for the 0.1, 1 mm, and 1 cm TRL.

(C) The optical performance comparison on the luminous reflectance at 60°C ($R_{um,60°C}$), luminous reflectance difference (ΔR_{lum}), IR reflectance difference (ΔR_{IR}), and solar reflectance difference (ΔR_{sol}) for the 0.1, 1 mm, and 1 cm TRL.

(D) Optical photos for 0.1 mm, 1 mm, and 1 cm sample at 20°C and 60°C, respectively.

(E) Specific heat capacity curve for TRL and DI water with respect to the temperature.

(F) FTIR spectrum for the TRL.

(G) Thermal conductivity curve for TRL and DI water with respect to the temperature.

high T_{lum} as the PNIPAm polymer fibers are thin and elongated to allow the light to pass though (Figure S1A). On the other hand, the transmittance of IR gradually decreases with the increasing of sample thickness. The IR transmittance (T_{IR}) for 0.1 mm sample is 77.0% at room temperature. With thickness increases, T_{IR} decreases to 67.0% and 47.3% for 1 mm and 1 cm sample, respectively. It is worth to mention that the absorption peak at 1,400 and 1,900 nm are due to the water molecules vibration in the TRL. However, when the thickness increased to 1 cm, because of the large thickness, the IR above 1,400 nm is absorbed.[21] When the temperature increases, the T_{lum} for all the samples decreases due to the shrinkage of PNIPAm polymer fibers and formation scattering center in TRL (Figure S1B). However, with the thickness increasing, ΔT_{sol} becomes larger. Figure S2 shows the hysteresis loop and the derivation of transmittance of the TRL against the temperature. It can be observed that the LCST is 32.5°C. Figures 2B and 2C summarize the optical properties for different thickness samples. It can be observed that the transmittance modulation abilities for luminous, IR, and solar wavelength are all increasing with the increase of thickness (Figure 2B). For example, the ΔT_{lum} of 0.1-mm sample is ~15%, and it increases significantly to ~90% for the 1-cm sample. Meanwhile, the ΔT_{sol} of 0.1-mm TRL is only 11.3%, and it largely increases to 68.1% for 1-cm TRL. Therefore, the 1-cm sample shows a higher transmittance contrast than the 1- and 0.1-mm samples. Similar to the transmittance modulation ability, the reflectance modulation ability becomes stronger when the sample becomes thicker (Figures 2C and S3). Moreover, the 1-cm sample shows a higher solar reflectance (R_{sol}, ~27%) than the other samples (~23% for 1-mm sample and ~10% for 0.1-mm sample, respectively), which indicates that the 1-cm sample shows stronger reflection to solar light in the opaque state. The effect of PNIPAm concentration to the thermochromic properties of TRL was further investigated. It can be observed that T_{lum} of 1-cm TRL decreases from 92.3% to 87.3% when the PNIPAm concentration increases from 0.1% to 20% (Figure S4A); while the maximum value of ΔT_{sol} was observed with 4% PNIPAm TRL (68.1%, Figure S4B).

Figure 2D shows the optical photos for different thickness samples at 20°C and 60°C. The optical photos agree with the spectra: at low temperature, all the samples are transparent, the luminous transmittance will not be affected by thickness. On the other hand, when the temperature is above LSCT, no significant transmittance change is observed for the 0.1-mm sample. In contrast, the 1-mm sample becomes translucent, and the 1-cm sample turns opaque, while the flower under the 1-cm sample becomes invisible. Thus, the thermo-responsive optical properties of the TRL were regulated by changing temperature and thickness.

Figure 2E shows the curve of C_p with respect to the temperature increase for the TRL and deionized (DI) water. No significant change of C_p is observed from 20°C to 80°C for both TRL and DI water. Moreover, the liquid shows a higher C_p (~4.35 kJ kg^{-1} K^{-1}) than that of DI water (~4.2 kJ kg^{-1} K^{-1}), while water has significantly higher C_p compared with most of the other materials (Table S1). As the large C_p of water is mainly attributed to the presence of hydrogen bond, the increasing of C_p is due to the introduction of the functional group (amide group and –C=O bond) for the liquid (Figures 2F and S5), which will generate more hydrogen bond and stabilize the water-water hydrogen bond.[57,65,66] Therefore, although the latent heat during the phase change at 32°C is negligible (Figure S6), the high C_p of TRL makes it is able to store larger amount of thermal energy than conventional building materials and glass with the same amount of temperature change. As the result, TRL becomes a competitive candidate for energy storage material to regulate the room temperature. Meanwhile, Figure 2G shows the relationship between thermal conductivity and the temperature changes of TRL and DI water. The thermal conductivities are stable at the temperature range from 20°C to 80°C for both liquids. It is worth mentioning that the thermal conductivities of both TRL (0.85W m^{-1} K^{-1}) and DI water (0.65 W m^{-1} K^{-1}) are higher than the commonly used TES materials, such as paraffin (0.18–0.19 W m^{-1} K^{-1}), fatty acids (0.14–0.37 W m^{-1} K^{-1}), and inorganic salt ($Na_2HPO_4 \cdot 12H_2O$, 0.47–0.51 W m^{-1} K^{-1}).[67] As a lower thermal conductivity will reduce the energy charging/discharging rate, thereby further reducing the energy storage efficiency of the material, the high thermal conductivity of the TRL makes the temperature distribution of window more uniform and provides the window with higher energy storage efficiency.[67–69] Moreover, the TRL has a viscosity that comparable to water (TRL: 1.80 cP, water: 1.05 cP); which provides its capability of easy fabrication.

HTEST Smart Window Design and Energy-Saving Demonstration

From the discussion above, the TRL shows an excellent light regulating ability as well as a good energy storage property. The working principles under different conditions for the HTEST smart window are described in Figure 3A. During the morning and evening in summer, the ambient temperature is not high enough to trigger the phase change of the HTEST window. Therefore, the light (yellow arrows in Figure 3A) will transmit to the room, and the window will keep the transparent state. Meanwhile, the artificial lighting electricity can be saved in the morning due to the sufficient daylighting penetration. Meanwhile, because of the good energy storage property of the TRL, the heat (red arrows in Figure 3A) in the surrounding is difficult to transfer into the room. As a result, the room will be kept at a relatively low temperature. Approaching noon in summer, the outdoor temperature reaches the maximum value of the day, which is above the LCST for the HTEST smart window. The phase change is subsequently activated, and the window becomes translucent/opaque to prevent the sunlight from further heating up the room. Meanwhile, the heat is further stored in the TRL and prevented from entering the room. The heat stored in the liquid is subsequently released, which shifts the peak of the cooling load. On the other hand, the window will keep transparent for the whole day in winter to ensure that the sunlight is able to transmit into the room for heating and lighting purpose. Based on such a working principle, the HTEST smart window is capable of reducing the HVAC energy consumption of buildings through cutting off the energy loss for cooling and increase the thermal comfort of the residence. In order to further investigate the performance of the HTEST smart window, the indoor thermal test was conducted as the proof of concept.

The indoor thermal test was designed to explore the solar modulation and TES effects of TRL energy-saving performance. Figure 3B shows the illustration of the experimental setup for the indoor thermal test, which is to test the solar modulation and TES effects on energy saving. Four samples namely normal glass panel (as baseline), 1 cm DI water trapped glass panel, 1 mm and 1 cm TRL trapped glass panel was installed onto four glasshouses (20 cm × 20 cm × 30 cm) to study the temperature change. In order to investigate the energy-saving ability of HTEST smart window more systematically, the PNIPAm particles concentration of 1-mm-thick sample were increased to make it have the similar solar transmittance and optical response ($T_{sol\text{-}1mmTRL}$ = 3.7%) as the 1-cm-thick sample ($T_{sol\text{-}1cmTRL}$ = 1.6%) (Figures 3C and S7), which gives large contrast with the other sets of sample, glass ($T_{sol\text{-}glass}$ = 85%) and 1 cm water ($T_{sol\text{-}1cmwater}$ = 72%) samples. During the test, the temperature of the inner surface of the window (position A), and the air temperature of the geometry center of the box (position B) were recorded, respectively. Figure 3D shows the temperature curve at position A for the four samples. The 1-mm-thick-liquid-trapped window and the normal glass show the highest surface temperature of 90°C and 88°C among the four samples. The temperatures recorded for 1-cm-thick water and 1-cm TRL samples are 46°C and 42°C, respectively. More than 40°C temperature difference was observed on the two sets of samples. As the inner surface temperature of the window is mainly affected by the heat accumulated on the window and the heat transferred through the window, the large difference between the C_p of water and glasses (4.2 versus 0.84 kJ kg^{-1} K^{-1}) indicated that the heat accumulated through the solar radiation is stored more in the water richer material. Thereby, a largely reduced surface temperature was detected on the thicker (1 cm) samples, as thicker samples provide more TES.[31]

Figure 3E describes the relationship between air temperature (position B) and the irradiating time for the four glasshouses. Before switching off the light of solar

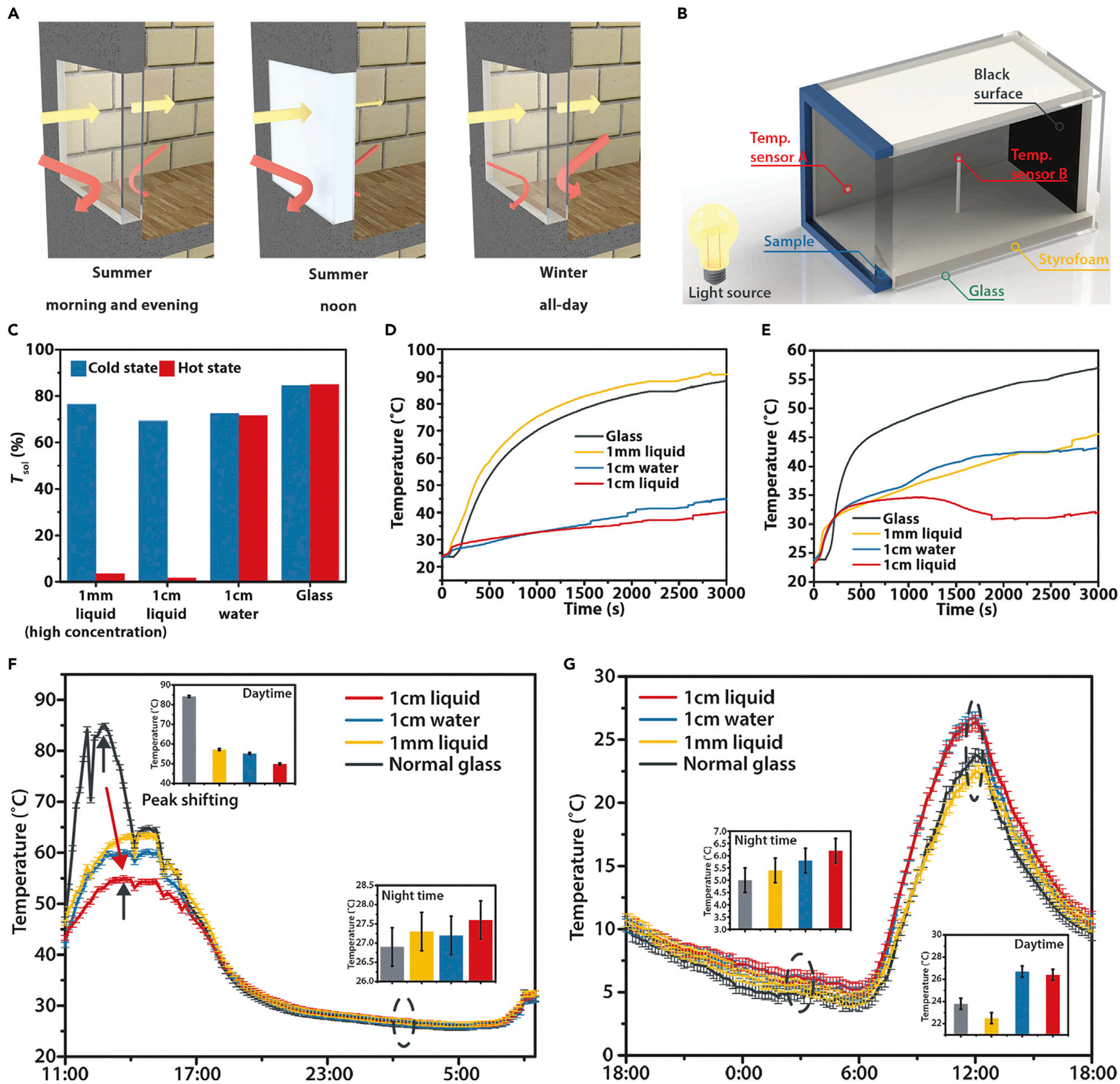

Figure 3. Energy-Saving Demonstration of HTEST Smart Window

(A) Working principles for the HTEST smart window in summer morning and evening, summer noon, and winter, respectively.

(B) Scheme of the indoor thermal test set up for HTEST smart window.

(C) Tsol for 1-mm TRL (high concentration), 1-cm TRL, 1-cm water, and normal glass at 20°C (cold state) and 60°C (hot state), respectively.

(D) Temperature of the inner surface of the window (temperature reading of sensor A) with respect to the lighting time for the glass panel, 1-mm liquid (high concentration), 1-cm water, and 1-cm liquid, respectively. The error bar for the temperature reading is $\pm$ 0.5°C due to the system errors of thermocouple.

(E) Air temperature in the box (temperature reading of sensor B) with respect to the lighting time for the glass panel, 1-mm liquid (high concentration), 1-cm water, and 1-cm liquid, respectively. The error bar for the temperature reading is $\pm$ 0.5°C due to the system errors of thermocouple.

(F) 24-h air temperature curve for the outdoor demonstration in Singapore. The inserts are the daytime (12:00) and night (3:00) temperature reading for normal glass, 1-mm liquid, 1-cm water, and 1-cm liquid, respectively. The black arrows indicate the maximum temperature peak for the normal glass and the 1-cm TRL, respectively. The error bar for the temperature reading is $\pm$ 0.5°C due to the system errors of thermocouple.

(G) 24-h air temperature curve for the outdoor demonstration in Beijing. The inserts are the daytime (12:00) and night (3:00) temperature reading for normal glass, 1-mm liquid, 1-cm water, and 1-cm liquid, respectively. The error bar for the temperature reading is $\pm$0.5°C due to the system errors of thermocouple.

simulator, the highest air temperature of 57°C occurs in the box with normal glass; in contrast with 45°C for 1-mm TRL and 43°C for 1-cm water. More than 10°C reduction for 1-mm TRL sample compared with the normal glass panel is largely due to the much-reduced solar transmission (85.0% versus 3.7%) (Figure 3C). The 1-cm TRL has the lowest air temperature of 32°C, which is 9°C lower than the 1-cm water sample and the major reason is due to the large difference of T_{sol} (71.6%. versus 1.6%, Figure 3C) as they have the similar C_p, (4.2_{water} versus 4.35_{TRL} kJ kg^{-1} K^{-1}, Figure 2E). Meanwhile, the air temperature of 1-cm TRL sample is 11°C lower than that of the 1-mm TRL glasshouse. As the solar transmittance of both 1-mm- and 1-cm-thick samples are nearly the same above LCST (3.7%. versus 1.6%, Figure 3C), the large temperature difference between 1-mm and 1-cm TRL was mainly contributed by the high TES of the 1-cm-thick liquid as the TES is linearly proportional to the thickness.

Considering the small-size glass box used in the indoor test, the actual house energy consumption simulation with the climate of Shanghai was conducted (Figure S8). Using the energy consumption of normal glass (133 MJ m^{-2}) as a baseline, by fixing the optical response, 1-cm water (thermal storage capability) can reduce the energy consumption to 120 MJ m^{-2}; 1-mm TRL (optical modulation) could reduce to 119 MJ m^{-2}; 1-cm TRL (thermal storage capability + optical modulation) could further reduce the energy consumption to the lowest of 107 MJ m^{-2}. It can be concluded that solar transmission modulation together with high TES gives the best performance.

The 1-cm-thick TRL-filled window, the 1-mm-thick TRL-filled window, the 1-cm DI-water-filled window, and the normal glass window were subsequently applied for the outdoor demonstration. The outdoor tests of the HTEST smart window set up in the hot and cold environment were subsequently conducted, and the geometrical center air temperature was taken. The weather condition of outdoor experiments was listed in Table S2. Figure S9 shows the experiment set up in hot environment test conducted in Singapore. In the daytime of hot environment outdoor demonstration, in general, the normal glass window has the highest temperature, and the 1-cm TRL gives the lowest temperature from ~11:00 to ~18:00. At noon, the normal glass window has a house air temperature of 84°C, followed by 1-mm TRL (57°C), 1-cm water (55°C), and 1-cm TRL-filled window has the lowest house air temperature of 50°C (Figure 3F). Moreover, it is worth mentioning that the peak shifting is observed in the outdoor demonstration. Compared with the normal glass, the temperature peak of 1-cm TRL sample was shifted from ~12:00 to ~14:00, which is preferred to shift electricity usage to low utility price periods.[70] At night, the 1-cm HTEST window shows the comparable house air temperature of 28°C to the 1-cm water (27°C), 1-mm TRL (27°C), and normal glass (27°C). The outdoor demonstration conducted in Guangzhou also showed shifted peak and lowered daytime temperature (Figures S9 and S10).

The cold environment test was conducted in Beijing (Figure S9). As shown in Figure 3G, the 1-cm sample has the air temperature at night (6°C), which is comparable to 1-cm water (6°C), 1-mm TRL (5°C), and normal glass (5°C). Moreover, the TRL-filled tri-layered window has been compared with the air-filled tri-layered windows and the commercial heat blocking window film (3M™ Prestige70 with no smart functionality, Figure S11) to demonstrate its energy-saving performance. The results show that the TRL-filled glass has a lowered air temperature in the hot environment compared with both the air-filled one and the heat blocking film (Figures S11A and S11D). This is due to the much-reduced T_{sol} (6.5%) for TRL-filled window compared with those of air-filled (85%) and 3M™ Prestige70 (33.5%, Figure S11C).

Furthermore, in a cold environment, air-filled and TRL-filled windows give similar air temperatures. The durability of the HTEST smart window was evaluated by the cycling test. As shown in Figure S12, the transmittance of HTEST smart window at 650 nm at both 20°C and 60°C were almost constant after 100 cycles. Long-term stability of TRL was evaluated by accelerating test with Hallberg-Peck model which is derived from Arrhenius equation.[71] In 14 days of experiment, the changes of T_{lum} and ΔT_{sol} were recorded (Figure S13). With an accelerating factor of 459.96, the guaranteed lifetime of TRL is equal to 17.6 years, which is comparable to HfO_2-VO_2 multi-layer structure (~16 years)[72] and better than polymer-stabilized liquid crystal system (~8 years).[73]

Interestingly, the literature has proved that a 26-mm water layer is able to effectively reduce the airborne noise with the sound reduction index of 35 dB.[64] Since the TRL has very high water content, the HTEST smart window should have a high potential for the noise reduction application in buildings. The soundproof testing with 1-m^2 sample to mimic the actual situation of the building was subsequently conducted according to ISO 140-3 (Figure S14). Figure 4A shows the airborne sound reduction index of the HTEST window, the double-glazed window, and the normal glass window. It can be observed that the HTEST window show a better sound insulation property than both the double-glazed window and the normal glass window in the frequency range from 100 to 4,000 Hz. Meanwhile, the HTEST window shows a higher weighted sound reduction index (R_w, 39 dB for the HTEST window) than the double-glazed window and the normal glass window (34 and 30 dB, respectively).

Energy-Saving Performance Simulation of HTEST Smart Window

To investigate the energy-saving performance of HTEST smart window in the actual house design, an energy-saving simulation, which employs the actual-size building model was conducted. The house dimension is 8 m in length, 6 m in width, and 2.7 m in height, and the size of the window is 3 m in width and 2 m in height (Figure S15). By varying the number of windows with TES capability in the house, the volume ratio between the TES window and the house could be calculated. In this simulation, the optical responses were kept the same under all conditions and the only variable is the volume ratio. Figure S16 shows that the energy-saving effect contributed by TES capability is closely related to the volume ratio; the higher volume ratio gives the better energy-saving capability. Subsequently, the weather data of Shanghai, Las Vegas, Riyadh, and Singapore were used for the simulation to identify the energy-saving potential of the HTEST smart window with different TRL thicknesses (1 mm and 1 cm); and using the normal glass window and low-E window as a comparison. Figures S17–S20 describes both the annual energy usage and the energy-saving potential of the four windows in the four cities, respectively. It is seen that the usage of HTEST smart windows decreased the HVAC energy consumption compared with both the normal glass window and the low-E window in all four cities. By deducting the energy consumption of normal glass windows, the annual HVAC energy savings of the 1-cm TRL, 1-mm TRL together with the low-E window in the four cities were plotted in Figure 4B. The 1-cm-TRL-filled window shows a better energy-saving performance than both the 1-mm TRL and the low-E window because of the combined large solar modulation capability as well as high TES capacity. Moreover, the HTEST smart window with 1-cm liquid can reduce 19.1%, 24.3%, 25.4%, and 44.6% of annual HAVC energy consumption compared with the normal glass window in Shanghai, Las Vegas, Riyadh, and Singapore, respectively. The simulation demonstrated that the 1-cm-liquid-trapped window is able to effectively save energy in actual buildings. Figures 4C–4F describe the monthly HVAC energy consumption of the four windows in Shanghai, Las Vegas, Riyadh, and Singapore,

Please cite this article in press as: Zhou et al., Liquid Thermo-Responsive Smart Window Derived from Hydrogel, Joule (2020), https://doi.org/10.1016/j.joule.2020.09.001

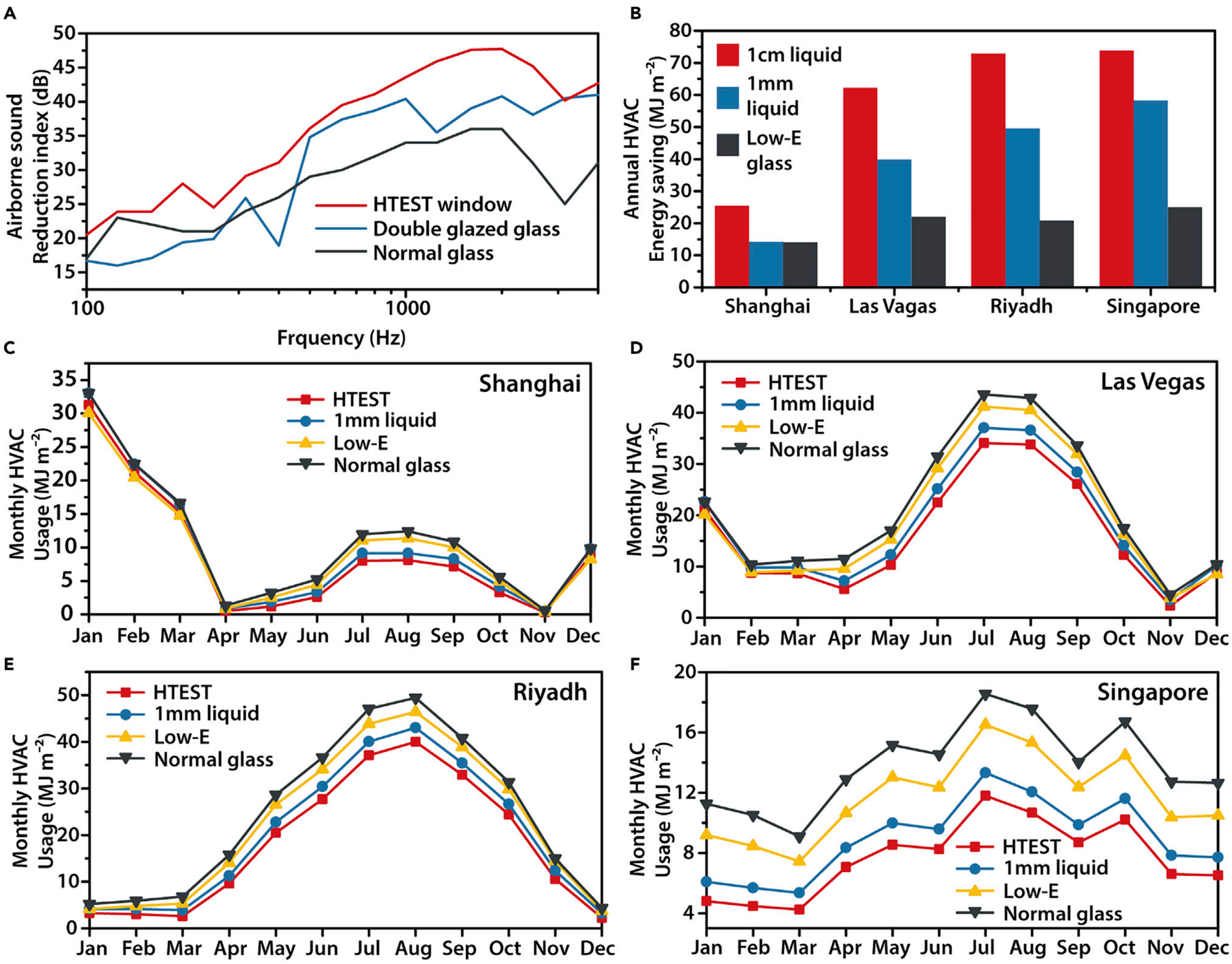

Figure 4. Energy-Saving Simulation and Soundproof Performance of HTEST Smart Window

(A) Airborne sound reduction index of HTEST window, double-glazed glass, and normal glass as the function of frequency.

(B) Annual HVAC energy-saving performance of the 1-cm-liquid-filled smart window, the 1-mm-TRL-filled smart window, and the low-E window with regard to the normal glass window in the climate condition of Shanghai, Las Vegas, Riyadh, and Singapore, respectively.

(C) Monthly HVAC energy consumption of the four types of windows in Shanghai.

(D) Monthly HVAC energy consumption of the four types of windows in Las Vegas.

(E) Monthly HVAC energy consumption of the four types of windows in Riyadh.

(F) Monthly HVAC energy consumption of the four types of windows in Singapore.

respectively. From April to November, the HTEST windows with 1-cm TRL showed better energy-saving performance than both the normal glass and the low-E windows in all four cities. The simulation results indicate that the HTEST smart window shows promising energy-saving performance in multiple cities.

In summary, in hot seasons, the HTEST window with 1-cm liquid shows superior energy-saving performance over the other types of windows. In cold seasons, the HTEST window shows a comparable energy-saving effect with the other types of windows in Shanghai and has better energy efficiency than the other windows in Las Vegas, Riyadh, and Singapore. Therefore, it can be concluded that the HTEST smart window shows satisfied energy-saving performance for actual buildings. Moreover, by conducting the annual daylighting simulation, it was found that the 1-cm HTEST smart window shows the highest useful daylight illuminance (UDI, 50% for

1-cm-liquid-filled HTEST window) compared with the 1-mm-liquid-filled window (36%) and the normal window (20%), which indicates that the HTEST smart window is able to improve the utilization of daylighting through proper solar transmittance regulation.[74]

DISCUSSION

A disruptive new window integrating the high energy storage intrinsic of water with the large solar modulation of thermo-responsive hydrogel was developed by trapping the hydrogel-derived TRL inside the double-glazed glass. The HTEST smart window with 1-cm TRL shows a high T_{lum} of 90% at room temperature and largely block the solar transmission when heated above LCST. Besides its outstanding transmission regulating ability (ΔT_{sol} = 68.1%), the TRL has a larger specific heat capacity (C_p, ~4.35 kJ kg^{-1} K^{-1}) than DI water (~4.2 kJ kg^{-1} K^{-1}), which is significantly higher than the commonly used TES and construction materials. For indoor thermal test, the sample with 1-cm liquid shows temperature decreasing of 25°C, 13°C, and 11°C compared with the normal glass panel, 1-cm-water-trapped glass and 1-mm-TRL-trapped glass, indicating that the thermal storage capability together with the solar modulation gives the best energy-saving potentials. Compared with 1-cm water, 1-mm liquid, and normal glass in the outdoor demonstrations, the lowered daytime air temperature in a hot environment, and the comparable night-time air temperature in cold weather was observed for the 1-cm-TRL-trapped HTEST smart window. The HVAC energy consumptions in Shanghai, Las Vegas, Riyadh, and Singapore were calculated via energy-saving simulations. The results show that the HTEST smart window with 1-cm TRL (highest solar modulation ability and TES) has the most promising annual energy-saving performance in all four cities compared with the other glass panels. Although this is a completely new concept of the glass panel, one of the potential issues is the leakage and drying of water between glass panels. The possible solutions could be encapsulating inside plastic or designing new glass panel structures, but much further work needs to be done to solve the issue. Moreover, anti-freezing additives could be mixed with TRL in order to lower the freezing point of TRL and extend the application range of HTEST window in colder region. The free-flow characteristic of the liquid trapped between glasses gives the unique advantages of easy fabrication and scaleup, high uniformity, and no constraint of glass shape and size, which makes it highly promising to commercialization. This revolutionary technology has the high potential to cut down the carbon emission and improve the sustainability of buildings and greenhouses.

EXPERIMENTAL PROCEDURES

Resource Availability

Lead Contact

Further information and requests for resources and reagents should be directed to and will be fulfilled by the Lead Contact, Yi Long (longyi@ntu.edu.sg).

Materials Availability

This study did not generate new unique reagents.

Data and Code Availability

This study did not generate or analyze datasets or code.

Materials

N-isopropylacrylamide (NIPAm, 98%, Wako Pure Chemical Industries Ltd), N,N-methylenebis (acrylamide) (99%, crosslinker, Sigma-Aldrich), N,N,N,N-tetramethylethylenediamine (TEMED, accelerator, 99%, Sigma-Aldrich), ammonium peroxydisulfate (initiator, 98%, Alfa Aesar), and 1-mm-thick double-sided closed-cell acrylic foam tape (3M™ VHB™ tape) were used without further purification. DI water was used throughout the experiments. Five transparent glass boxes of dimension 30 cm × 20 cm × 20 cm (L × W × H) and 2-cm-thick styrofoam were used for indoor and outdoor testing.

Preparation of PNIPAm TRL and High-Concentration TRL

3.164 g (0.14 mol) of NIPAm monomer and 862.4 mg (0.028 mol) of the crosslinker (acrylamide) were dissolved in DI water at 25°C to make 400 mL homogeneous aqueous solution. Then, 6.15 mL of TEMED (catalyst) was added, followed by mixing at 600 rpm for 30 min. Finally, 12.3 mL of APS (initiator) was added to the solution. In order for the reaction to be completed, the solution was left stirring for at least 24 h. The whole procedure (including completion of the reaction) was conducted at room temperature (25°C) (Figure S21). Then, the homogeneous liquid underwent a pre-freezing process by liquid nitrogen, followed by the freeze-drying vacuum at −50°C for 72 h. After freeze-drying, the PNIPAm powder was directly dispersed into 100 mL DI water by using vortex for 30 min; then the PNIPAm TRL was made. The preparation of high concentration liquid has the same procedure as the normal PNIPAm TRL, repeat the procedure of making PNIPAm powder, and dispersed the powder in 20-mL DI water by using vortex for 30 min.

Preparation of Samples for Indoor Thermal Test, HTEST Smart Window, and Large-Scale Smart Window

The high concentration liquid was poured directly into the prepared simple glass box with 1 mm reserved space to form the 1-mm high-concentration liquid sample (Figure S22), which was then sealed with silicone gel. The size of all samples was 20 × 20 cm. Similarly, the normal PNIPAM liquid and DI water were poured directly into the prepared glass boxes (20 × 20 cm) with 1-cm-thick reserved space to form 1-cm water sample and 1-cm liquid sample, respectively. The glass box was then sealed with silicone gel. For the large-scale sample, the PNIPAM TRL filled half of the double-glazed glass box (50 × 100 cm).

Characterization

The transmittance and reflectance spectra were collected on a UV-vis-NIR spectrophotometer system with the integration sphere attached (AvaSpec-ULS2048L StarLine Versatile Fiber-optic spectrometer and AvaSpec-NIR256-2.5-HSC-EVO, Avantes, the Netherlands). The spectrophotometer is equipped with a heating and cooling stage (PE120, Linkam, UK).

The T_{lum}, T_{IR} and solar transmittance T_{sol} were calculated by Equation 1[75]

$$T_{lum/IR/sol} = \int \phi_{lum/IR/sol} T(\lambda) d\lambda \Big/ \int \phi_{lum/IR/sol} d\lambda \qquad \text{(Equation 1)}$$

where $T(\lambda)$ denotes spectral transmittance, $\psi_{lum}(\lambda)$ is the standard luminous efficiency function of photopic vision in the wavelength range of 380–780 nm,[76] $\psi_{IR}(\lambda)$ and $\psi_{sol}(\lambda)$ are the IR/solar irradiance spectra for air mass 1.5 (corresponding to the sun standing 37° above the horizon with 1.5-atmosphere thickness, corresponds to a solar zenith angle of 48.2°), respectively.[77] The images of PNIPAm polymer fiber at 20°C and 60°C were taken by scanning electron microscope (SEM, Carl Zeiss Supra 55).

The specific heat capacity and thermal conductivity of TRL are characterized with thermal conductivity analyzer equipped with the modified transient plane source

(MTPS) sensor (TCi, C-Therm Technologies Ltd.). The system is in a thermal chamber (TJR CE-NY-WF4, Thermal Product Solutions).

The viscosity of TRL and DI water were measured by a viscometer (Brookfield LV DV3T, with a CP-42Z spindle installed) at 25°C. The rotation speed of spindle was set at 20 rpm (shear rate 76.80 S^{-1}). The data were recorded through single point averaging mode with a recording time of 10 s.

The cycling test was conducted on the same UV-vis-NIR spectrometer system for the transmittance and reflection spectra measurement. The TRL was heated to the 60°C and then cooled down back to 20°C as a testing cycle, and 100 cycles were conducted. The transmittance at 650 nm at 20°C and 60°C for every cycle is recorded for the durability analysis.

Indoor Thermal Test Procedure

Indoor thermal testing is a proof of concept of the TRL, which can both regulate solar light and store heat energy. This test provides a controlled environment for the experiment without temperature fluctuation and compares 4 samples: glass panel, 1-mm-thick liquid, 1-cm-thick DI water, and 1-cm-thick liquid. Through this testing, it provides an accurate assessment of the TRL effectiveness. The indoor lighting testing environment temperature is 24°C. The indoor test glass box was fabricated by one glass box, five pieces of 2-cm-thick styrofoam with a black inner face, and different samples. Thermocouples were used to detect the temperature of 2 different parts in the glass box: the inner surface of the window (temperature sensor A) and air temperature at the geometrical center inside the box (temperature sensor B). The dimension of the glass box was measured (20 × 20 × 30 cm), and styrofoam was cut and used to align the sides and back. The experimental setup is showed in Figure 3B.

The solar light with the power of 500 W used in the experiment was placed 25 cm away from the front of the glass box. The area between the lamp and the glass box was connected with an aluminum foil to prevent heat loss. An electric fan was placed approximately 50 cm away from the glass box for reduction of temperature after the solar light was switched off. Agilent BenchLink Data Logger 3 software for temperature measurement was used to collect data.

Outdoor Test Procedure

The outdoor test was designed to compare the energy-saving performance of glass panel, 1-mm-thick liquid, 1-cm-thick DI water, and 1-cm-thick liquid samples. It provides a realistic experiment environment with temperature fluctuation. A box (inner dimension: 20 cm × 20 cm × 30 cm) with glass panel (glass thickness is 5 mm, dimension: 20 cm × 20 cm) on the top was set as a control sample with thermocouple sensors in the geometrical center. The rest of testing setup has the same design as the control sample, while the glass panel was replaced by 1-mm-thick liquid, 1-cm-thick DI water, and 1-cm-thick liquid, respectively. For the outdoor demonstration in hot temperature, the four setups were placed outdoor without any shelter and subjected to direct sunlight. The data were recorded every 10 min in Singapore and Guangzhou. For the demonstration in cold temperature, four 10-W heaters were placed in the geometrical center of the testing box as the heating sources. The cold environment demonstration was conducted in Beijing, and the data were recorded every 10 min in 24 h. The weather information of Singapore, Guangzhou, and Beijing at the date of experiment were summarized in Table S3. As the temperature recorded by thermocouple has a ~1°C system error, the ±0.5°C was added to the temperature reading.

Acceleration Experiment Procedure

The acceleration experiment was conducted with Hallberg-Peck model, which is derived from the Arrhenius equation.[71] The formula that calculate the acceleration factor was given by equation 2:

$$AF = exp\left[\frac{E_a}{k} * \left(\frac{1}{T_{use}} - \frac{1}{T_{test}}\right)\right] * \left(\frac{RH_{test}}{RH_{use}}\right)^n \qquad \text{(Equation 2)}$$

where AF was the acceleration factor. E_a was the activation energy of PNIMAm (0.81 eV).[78] k is Boltzmann's constant. T_{use} and T_{test} were the operating temperature (298 K) and test temperature (353 K in this work), respectively. RH_{test} and RH_{use} are relative humidity of test (90%) and relative humidity in operation (60%), respectively. According to the model, the value of n was set to 3.[71] By substituting the experiment condition and constant into the formula, the acceleration factor was calculated as 459.96.

Energy-Saving Potential Assessment of HTEST Smart Window

The energy efficiency assessment can be divided into the following steps:

Step 1: Window Modeling

The HTEST smart window model was established in WINDOW software and another two windows: normal glass window and low-E window have been modeled for comparison. The thermal properties include U-factor and solar heating gain coefficient (SHGC) of the normal glass window, low-E window, 1-mm-liquid-filled window, and 1-cm-liquid-filled window were listed in Table S3.

Step 2: Building Modeling

The building model in Figure S15 was used for the energy-saving simulation. Since the WINDOW software was unable to calculate window with TES materials, some equivalent processing has been done. The heat capacity of the HTEST window was equivalent to the wall where the window was located to determine the energy efficiency of the HTEST window. Besides, the heat transfer coefficient of the wall was adjusted to be the same as the HTEST window to ensure that the portion of the heat absorbed into the chamber is the same.

Step 3: Energy Simulation

The climate data of Singapore, Shanghai, Las Vegas, and Riyadh were selected as the simulation environment data. The dimension of the building model is 8 m in length, 6 m in width, and 2.7 m in height. Same windows (3 m in width and 2 m in height) are arranged in the four orientations to avoid the impact of orientation. The parameter settings of the building envelope are according to the local building energy efficiency standards and the four walls are all exterior walls. The air-conditioning system used for cooling-dominated climates is heat pump only, and for heating-dominated climates heat pump and boiler. Electricity used for cooling and natural gas used for heating is both converted to primary energy for a unified comparison. Since the characteristics of the liquid changed due to temperature, for annual HVAC energy simulation, the hot period used the optical and thermal properties at high temperatures, and the cold period uses the optical and thermal properties at low temperature. The energy-saving simulation result for the four windows was then compared to calculate the energy-saving potential.

SUPPLEMENTAL INFORMATION

Supplemental Information can be found online at https://doi.org/10.1016/j.joule.2020.09.001.

ACKNOWLEDGMENTS

The Principal Investigator of this project (Y.L.) wishes to thank Sino-Singapore International Joint Research Institute for funding support. This research was supported by Singapore Ministry of Education (MOE) Academic Research Fund Tier one RG103/19 and the National Research Foundation, Prime Minister's Office, Singapore under its Campus for Research Excellence and Technological Enterprise (CREATE) program. Y.Z. and Y.L. sincerely thank the generous funding support from Prof. Freddy Y.C. Boey.

AUTHOR CONTRIBUTIONS

Y.L. proposed, designed, and guided the project and revised the manuscript. Y.Z. and S.W. contributed equally to this work, performed most of the experiments, and drafted the manuscript. J.P. guided and Y.T. performed the building energy simulation. C.L. and F.Y.C.B. polished and revised the manuscript. All authors checked the manuscript.

DECLARATION OF INTERESTS

The authors declare no competing interests.

Received: February 27, 2020
Revised: May 18, 2020
Accepted: August 31, 2020
Published: September 23, 2020

REFERENCES

1. Masson-Delmotte, V. (2018). Global Warming of 1.5 °C: an IPCC Special Report on the Impacts of Global Warming of 1.5° C Above Pre-Industrial Levels and Related Global Greenhouse Gas Emission Pathways. the Context of Strengthening the Global Response to the Threat of Climate Change, Sustainable Development, and Efforts to Eradicate Poverty (World Meteorological Organization).
2. Ke, Y., Zhou, C., Zhou, Y., Wang, S., Chan, S.H., and Long, Y. (2018). Emerging thermal-responsive materials and integrated techniques targeting the energy-efficient smart window application. Adv. Funct. Mater. *28*, 1800113.
3. Wang, S., Owusu, K.A., Mai, L., Ke, Y., Zhou, Y., Hu, P., Magdassi, S., and Long, Y. (2018). Vanadium dioxide for energy conservation and energy storage applications: synthesis and performance improvement. Appl. Energy *211*, 200–217.
4. Gao, Y., Wang, S., Kang, L., Chen, Z., Du, J., Liu, X., Luo, H., and Kanehira, M. (2012). VO2–Sb:SnO2 composite thermochromic smart glass foil. Energy Environ. Sci. *5*, 8234–8237.
5. Hee, W.J., Alghoul, M.A., Bakhtyar, B., Elayeb, O., Shameri, M.A., Alrubaih, M.S., and Sopian, K. (2015). The role of window glazing on daylighting and energy saving in buildings. Renew. Sustain. Energ. Rev. *42*, 323–343.
6. Kalnæs, S.E., and Jelle, B.P. (2015). Phase change materials and products for building applications: a state-of-the-art review and future research opportunities. Energ. Build. *94*, 150–176.
7. Granqvist, C.G., Lansåker, P.C., Mlyuka, N.R., Niklasson, G.A., and Avendaño, E. (2009). Progress in chromogenics: new results for electrochromic and thermochromic materials and devices. Sol. Energy Mater. Sol. Cells *93*, 2032–2039.
8. Warwick, M.E.A., and Binions, R. (2014). Advances in thermochromic vanadium dioxide films. J. Mater. Chem. A *2*, 3275–3292.
9. Granqvist, C.G. (2007). Transparent conductors as solar energy materials: a panoramic review. Sol. Energy Mater. Sol. Cells *91*, 1529–1598.
10. Cui, Y.Y., Ke, Y., Liu, C., Wang, N., Chen, Z., Zhang, L.M., Zhou, Y., Wang, S., Gao, Y.F., and Long, Y. (2018). Thermochromic VO2 for energy-efficient smart windows. Joule *2*, 1707–1746.
11. Ke, Y., Zhang, Q., Wang, T., Wang, S., Li, N., Lin, G., Liu, X., Dai, Z., Yan, J., Yin, J., et al. (2020). Cephalopod-inspired versatile design based on plasmonic VO2 nanoparticle for energy-efficient mechano-thermochromic windows. Nano Energy *73*, 104785.
12. Tang, L., Wang, L., Yang, X., Feng, Y., Li, Y., and Feng, W. (2021). Poly(N-isopropylacrylamide)-based smart hydrogels: design, properties and applications. Prog. Mater. Sci. *115*, 100702.
13. Gutierrez-Cuevas, K.G., Wang, L., Zheng, Z.G., Bisoyi, H.K., Li, G., Tan, L.S., Vaia, R.A., and Li, Q. (2016). Frequency-driven self-organized helical superstructures loaded with mesogen-grafted silica nanoparticles. Angew. Chem. Int. Ed. Engl. *55*, 13090–13094.
14. Dong, L., Feng, Y., Wang, L., and Feng, W. (2018). Azobenzene-based solar thermal fuels: design, properties, and applications. Chem. Soc. Rev. *47*, 7339–7368.
15. Wang, L., Bisoyi, H.K., Zheng, Z., Gutierrez-Cuevas, K.G., Singh, G., Kumar, S., Bunning, T.J., and Li, Q. (2017). Stimuli-directed self-organized chiral superstructures for adaptive windows enabled by mesogen-functionalized graphene. Mater. Today *20*, 230–237.
16. Liu, C., Cao, X., Kamyshny, A., Law, J.Y., Magdassi, S., and Long, Y. (2014). VO2/Si-Al gel nanocomposite thermochromic smart foils: largely enhanced luminous transmittance and solar modulation. J. Colloid Interface Sci. *427*, 49–53.
17. Seeboth, A., Ruhmann, R., and Mühling, O. (2010). Thermotropic and thermochromic

polymer based materials for adaptive solar control. Materials *3*, 5143–5168.

18. Ke, Y., Wang, S., Liu, G., Li, M., White, T.J., and Long, Y. (2018). Vanadium dioxide: the multistimuli responsive material and its applications. Small *14*, e1802025.

19. Ke, Y., Chen, J., Lin, G., Wang, S., Zhou, Y., Yin, J., Lee, P.S., and Long, Y. (2019). Smart windows: electro-, thermo-, mechano-, photochromics and beyond. Adv. Energy Mater. *9*, 1902066.

20. Li, L., Yu, H., and Liu, R. (2017). Research on composite-phase change materials (PCMs)-bricks in the west wall of room-scale cubicle: mid-season and summer day cases. Building and Environment *123*, 494–503.

21. Zhou, G., and He, J. (2015). Thermal performance of a radiant floor heating system with different heat storage materials and heating pipes. Appl. Energy *138*, 648–660.

22. Saffari, M., Piselli, C., de Gracia, A., Pisello, A.L., Cotana, F., and Cabeza, L.F. (2018). Thermal stress reduction in cool roof membranes using phase change materials (PCM). Energ. Build. *158*, 1097–1105.

23. Zhu, N., Li, S., Hu, P., Wei, S., Deng, R., and Lei, F. (2018). A review on applications of shape-stabilized phase change materials embedded in building enclosure in recent ten years. Sustain. Cities Soc. *43*, 251–264.

24. Song, M., Niu, F., Mao, N., Hu, Y., and Deng, S. (2018). Review on building energy performance improvement using phase change materials. Energ. Build. *158*, 776–793.

25. Gil, A., Medrano, M., Martorell, I., Lázaro, A., Dolado, P., Zalba, B., and Cabeza, L.F. (2010). State of the art on high temperature thermal energy storage for power generation. Part 1—concepts, materials and modellization. Renew. Sustain. Energ. Rev. *14*, 31–55.

26. Sharma, A., Tyagi, V.V., Chen, C.R., and Buddhi, D. (2009). Review on thermal energy storage with phase change materials and applications. Renew. Sustain. Energ. Rev. *13*, 318–345.

27. Kuznik, F., David, D., Johannes, K., and Roux, J.J. (2011). A review on phase change materials integrated in building walls. Renew. Sustain. Energ. Rev. *15*, 379–391.

28. Cabeza, L.F., Gutierrez, A., Barreneche, C., Ushak, S., Fernández, Á.G., Inés Fernádez, A.I., and Grágeda, M. (2015). Lithium in thermal energy storage: a state-of-the-art review. Renew. Sustain. Energ. Rev. *42*, 1106–1112.

29. Gutierrez, A., Miró, L., Gil, A., Rodríguez-Aseguinolaza, J., Barreneche, C., Calvet, N., Py, X., Inés Fernández, A.I., Grágeda, M., Ushak, S., and Cabeza, L.F. (2016). Advances in the valorization of waste and by-product materials as thermal energy storage (TES) materials. Renew. Sustain. Energ. Rev. *59*, 763–783.

30. Pielichowska, K., and Pielichowski, K. (2014). Phase change materials for thermal energy storage. Prog. Mater. Sci. *65*, 67–123.

31. Tipler, P.A., and Mosca, G. (2007). Physics for Scientists and Engineers (MacMillan).

32. Hasan, M.I., Basher, H.O., and Shdhan, A.O. (2018). Experimental investigation of phase change materials for insulation of residential buildings. Sustain. Cities Soc. *36*, 42–58.

33. Luo, R., Wang, S., Wang, T., Zhu, C., Nomura, T., and Akiyama, T. (2015). Fabrication of paraffin@SiO2 shape-stabilized composite phase change material via chemical precipitation method for building energy conservation. Energ. Build. *108*, 373–380.

34. Koschenz, M., and Lehmann, B. (2004). Development of a thermally activated ceiling panel with PCM for application in lightweight and retrofitted buildings. Energ. Build. *36*, 567–578.

35. Kant, K., Shukla, A., and Sharma, A. (2017). Heat transfer studies of building brick containing phase change materials. Sol. Energy *155*, 1233–1242.

36. Kong, W., Liu, Z., Yang, Y., Zhou, C., and Lei, J. (2017). Preparation and characterizations of asphalt/lauric acid blends phase change materials for potential building materials. Constr. Build. Mater. *152*, 568–575.

37. Linstrom, P.J., and Mallard, W.G. (2019). NIST Chemistry WebBook-NIST Standard Reference Database Number 69 (National Institute of Standards and Technology), p. 20899.

38. Tang, F., Cao, L., and Fang, G. (2014). Preparation and thermal properties of stearic acid/titanium dioxide composites as shape-stabilized phase change materials for building thermal energy storage. Energ. Build. *80*, 352–357.

39. Lide, D.R. (2009). CRC Handbook of Chemistry and Physics (CRC Press).

40. Evers, A.C., Medina, M.A., and Fang, Y. (2010). Evaluation of the thermal performance of frame walls enhanced with paraffin and hydrated salt phase change materials using a dynamic wall simulator. Building and Environment *45*, 1762–1768.

41. Berroug, F., Lakhal, E.K., El Omari, M., Faraji, M., and El Qarnia, H. (2011). Thermal performance of a greenhouse with a phase change material north wall. Energ. Build. *43*, 3027–3035.

42. Pasupathy, A., Athanasius, L., Velraj, R., and Seeniraj, R.V. (2008). Experimental investigation and numerical simulation analysis on the thermal performance of a building roof incorporating phase change material (PCM) for thermal management. Appl. Therm. Eng. *28*, 556–565.

43. Rgees, L. (2014). PCM-OM55P product data sheet. https://rgees.com/documents/Data%20Sheets/savENRG%20PCM%20OM55P.pdf.

44. PlusICE PCM (organic) (A) range, . http://www.pcmproducts.net/files/PCM%20Summary%202013-A.pdf.

45. PCM Energy P. Ltd (2019). Phase change materials pcm manufacturers building & electronic air condition. http://pcmenergy.com/products.htm#Sseries30to45.

46. PCM Energy P. Ltd (2019). PlusICE PCM solid-solid (X) range. http://www.pcmproducts.net/files/PCM%20Summary%202013-X.pdf.

47. PX 25 data sheet. https://www.rubitherm.eu/media/products/datasheets/Techdata_-PX25_EN.PDF.

48. Incropera, F.P., and DeWitt, D.P. (2002). Fundamentals of Heat and Mass Transfer (J. Wiley).

49. Engineers edge (2020). Specific heat capacity of metals table. https://www.engineersedge.com/materials/specific_heat_capacity_of_metals_13259.htm.

50. E. ToolBox Specific heat of common Substances. https://www.engineeringtoolbox.com/specific-heat-capacity-d_391.htm.

51. Muthuraj, R., Lacoste, C., Lacroix, P., and Bergeret, A. (2019). Sustainable thermal insulation biocomposites from rice husk, wheat husk, wood fibers and textile waste fibers: elaboration and performances evaluation. Ind. Crops Prod. *135*, 238–245.

52. Adl-Zarrabi, B., and Boström, L. (2004). Determination of thermal properties of wood and wood based products by using transient plane source. Proceedings of the 8th World Conference on Timber Engineering.

53. ASHRAE (1989). ASHRAE Handbook: Fundamentals (American Society of Heating, Refrigerating and Air-Conditioning Engineers).

54. Hasnain, S.M. (1998). Review on sustainable thermal energy storage technologies, part I: heat storage materials and techniques. Energy Convers. Manag. *39*, 1127–1138.

55. Zhou, Y., Cai, Y., Hu, X., and Long, Y. (2014). Temperature-responsive hydrogel with ultra-large solar modulation and high luminous transmission for "smart window" applications. J. Mater. Chem. A *2*, 13550–13555.

56. Li, X.-H., Liu, C., Feng, S.-P., and Fang, N.X. (2019). Broadband light management with thermochromic hydrogel microparticles for smart windows. Joule *3*, 290–302.

57. Zhou, Y., Layani, M., Wang, S., Hu, P., Ke, Y., Magdassi, S., and Long, Y. (2018). Fully printed flexible smart hybrid hydrogels. Adv. Funct. Mater. *28*, 1705365.

58. Zhou, Y., Dong, X., Mi, Y., Fan, F., Xu, Q., Zhao, H., Wang, S., and Long, Y. (2020). Hydrogel smart windows. J. Mater. Chem. A *8*, 10007–10025.

59. Liu, J., An, T., Chen, Z., Wang, Z., Zhou, H., Fan, T., Zhang, D., and Antonietti, M. (2017). Carbon nitride nanosheets as visible light photocatalytic initiators and crosslinkers for hydrogels with thermoresponsive turbidity. J. Mater. Chem. A *5*, 8933–8938.

60. Owusu-Nkwantabisah, S., Gillmor, J., Switalski, S., Mis, M.R., Bennett, G., Moody, R., Antalek, B., Gutierrez, R., and Slater, G. (2017). Synergistic thermoresponsive optical properties of a composite self-healing hydrogel. Macromolecules *50*, 3671–3679.

61. La, T.G., Li, X., Kumar, A., Fu, Y., Yang, S., and Chung, H.J. (2017). Highly flexible, Multipixelated thermosensitive smart windows made of tough hydrogels. ACS Appl. Mater. Interfaces *9*, 33100–33106.

62. Zhou, Y., Cai, Y., Hu, X., and Long, Y. (2015). VO2/hydrogel hybrid nanothermochromic

material with ultra-high solar modulation and luminous transmission. J. Mater. Chem. A *3*, 1121–1126.

63. Zhou, Y., Wan, C., Yang, Y., Yang, H., Wang, S., Dai, Z., Ji, K., Jiang, H., Chen, X., and Long, Y. (2019). Highly stretchable, elastic, and ionic conductive hydrogel for artificial soft electronics. Adv. Funct. Mater. *29*, 1806220.

64. Wenmaekers, R., Van der Aa, B., Pronk, A., Couthinho, A., and van Luxemburg, L.C.J. (2008). The Sound insulation of water (34th German Conference on Acoustics).

65. Silverstein, K.A.T., Haymet, A.D.J., and Dill, K.A. (2000). The strength of hydrogen bonds in liquid water and around nonpolar solutes. J. Am. Chem. Soc. *122*, 8037–8041.

66. Tamai, Y., Tanaka, H., and Nakanishi, K. (1996). Molecular dynamics study of polymer−water interaction in hydrogels. 1. Hydrogen-bond structure. Macromolecules *29*, 6750–6760.

67. Fan, L., and Khodadadi, J.M. (2011). Thermal conductivity enhancement of phase change materials for thermal energy storage: a review. Renew. Sustain. Energ. Rev. *15*, 24–46.

68. Li, T.X., Xu, J.X., Wu, D.L., He, F., and Wang, R.Z. (2019). High energy-density and power-density thermal storage prototype with hydrated salt for hot water and space heating. Appl. Energy *248*, 406–414.

69. Yuan, K., Shi, J., Aftab, W., Qin, M., Usman, A., Zhou, F., Lv, Y., Gao, S., and Zou, R. (2020). Engineering the thermal conductivity of functional phase-change materials for heat energy conversion, storage, and utilization. Adv. Funct. Mater. *30*, 1904228.

70. Dahash, A., Ochs, F., Janetti, M.B., and Streicher, W. (2019). Advances in seasonal thermal energy storage for solar district heating applications: a critical review on large-scale hot-water tank and pit thermal energy storage systems. Appl. Energy *239*, 296–315.

71. Hallberg, Ö., and Peck, D.S. (1991). Recent humidity accelerations, a base for testing standards. Qual. Reliab. Engng. Int. *7*, 169–180.

72. Chang, T., Cao, X., Li, N., Long, S., Zhu, Y., Huang, J., Luo, H., and Jin, P. (2019). Mitigating deterioration of vanadium dioxide thermochromic films by interfacial encapsulation. Matter *1*, 734–744.

73. Hu, X., Zhang, X., Yang, W., Jiang, X.-F., Jiang, X., de Haan, L.T., Yuan, D., Zhao, W., Zheng, N., Jin, M., et al. (2020). Stable and scalable smart window based on polymer stabilized liquid crystals. J. Appl. Polym. Sci. *137*, 48917.

74. Nabil, A., and Mardaljevic, J. (2006). Useful daylight illuminances: a replacement for daylight factors. Energ. Build. *38*, 905–913.

75. Ke, Y., Yin, Y., Zhang, Q., Tan, Y., Hu, P., Wang, S., Tang, Y., Zhou, Y., Wen, X., Wu, S., et al. (2019). Adaptive thermochromic windows from active plasmonic elastomers. Joule *3*, 858–871.

76. Wyszecki, G., and Stiles, W.S. (2000). Color Science: Concepts and Methods, Quantitative Data and Fomulae (Wiley).

77. ASTM G173-03 (2012). Standard Tables of Reference Solar Spectral Irradiances: Direct Normal and Hemispherical on a 37 Tilted Surface (ASTM International). www.astm.org.

78. Hu, J., Chen, M., Tian, H., and Deng, W. (2015). Preparation and pyrolysis characteristics of PNIPAM-grafted SiO2 hollow spheres loading vitamin C. RSC Adv. *5*, 81134–81141.

JOUL, Volume *4*

Supplemental Information

Liquid Thermo-Responsive Smart Window Derived from Hydrogel

Yang Zhou, Shancheng Wang, Jinqing Peng, Yutong Tan, Chuanchang Li, Freddy Yin Chiang Boey, and Yi Long

Table S1. Specific heat capacity and TES performance with the temperature range of 10~70 °C for water, paraffin, fatty acid, inorganic PCMs, commercial PCMs, metal, glass, construction material, and wood.

Type of material	Name	Cp (kJ kg^{-1} K^{-1})	TES (kJ kg^{-1})	Reference
Water	Water	4.18	250.9	[31]
Paraffin	Paraffin wax	2.44 (Solid) 2.53 (Liquid)	322.9	[32]
	Paraffin	1.93 (Solid) 2.20 (Liquid)	372.0	[23]
	Paraffin	1.93 (Solid) 2.20 (Liquid)	307.5	[33]
	Hexadecane	1.65 (Solid) 2.10 (Liquid)	358.4	[34]
	Octadecane	1.75 (Solid) 2.10 (Liquid)	363.7	[34]
Fatty acid	Capric acid	1.90 (Solid) 2.40 (Liquid)	285.7	[35]
	Lauric acid	2.02 (Solid) 2.15 (Liquid)	296.8	[36, 37]
	Stearic acid	1.76 (Solid) 2.22 (Liquid)	298.6	[38, 39]
Inorganic PCMs	Hydrated salt	1.40 (Solid) 2.30 (Liquid)	295.9	[40]
	$CaCl_2{\cdot}6H_2O$	1.46 (Solid) 2.13 (Liquid)	302.56	[41]
	$CaCl_2$-NaCl-KCl-H_2O	1.44	274.4	[42]
Commercial PCMs	savENRG™ PCM-OM55P	0.73 (Liquid)	253.8	[43]
	PlusICE PCM Organic A32	2.20	262.0	[44]
	PCM Latest™ 36S	2.00	320.0	[45]
	PCM Latest™ 29T	2.00	308.0	[45]
	PlusICE PCM Solid-Solid X30	1.65	204.0	[46]

	PX 25	2.00	215.0	47
Metal	Steel	0.43	26.0	48
	Cast iron	0.46	27.6	49
	Brass	0.40	24.1	49
	Aluminum	0.92	55.3	49
Glass	Glass, silica	0.84	50.4	31
	Glass, crown	0.67	40.2	31
	Glass, flint	0.50	30.2	41
	Glass, Pyrex	0.75	45.2	23
Construction material	Brick	0.84	50.1	48
	Mortar	0.78	46.8	48
	Concrete	0.88	52.8	50
	Sand	0.83	49.8	50
Wood	Wood fiber board	0.83	49.6	51
	Low density fibre board	1.05	63.0	52
	Wood particle board	1.66	99.6	52
	Hard wood	1.63	97.8	53

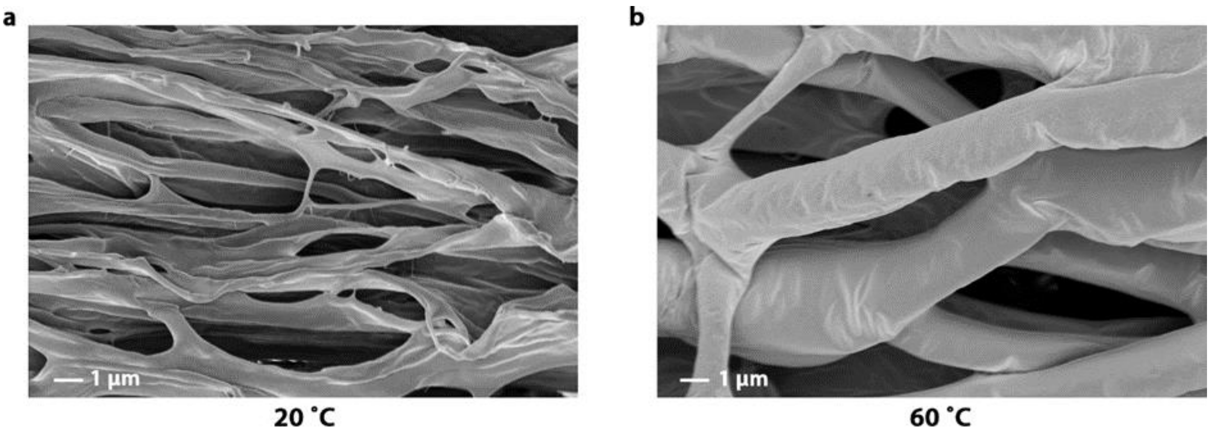

Figure S1. (a) SEM image of PNIPAm network structure at 20 °C. (b) SEM image of PNIPAm shrinkage network structure at 60 °C

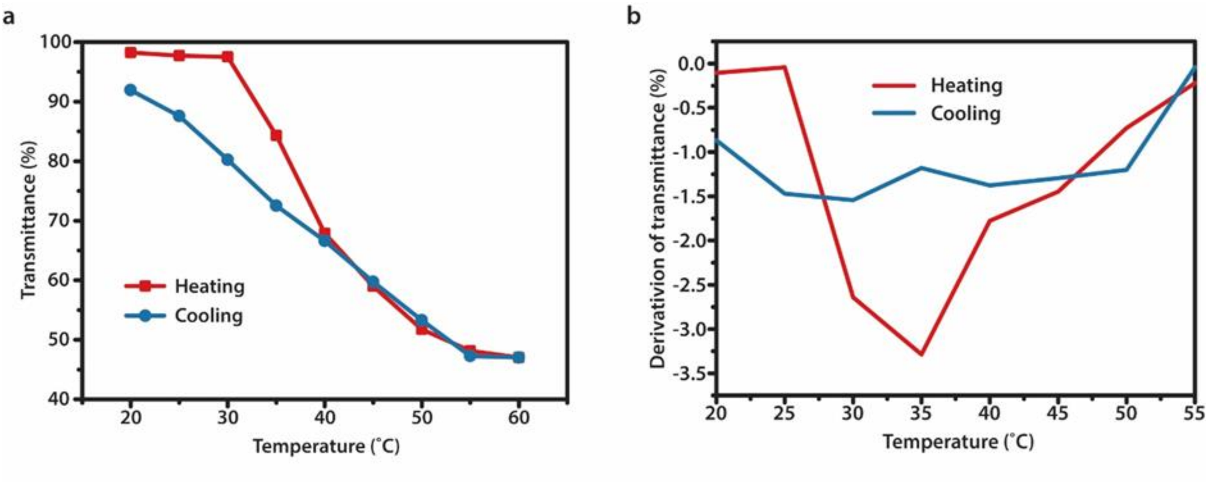

Figure S2. (a) Hysteresis loop for the transmittance at 650 nm to show the LCST of thermo-responsive liquid. (b) Transmittance derivation curves for the liquid during the heating and cooling process.

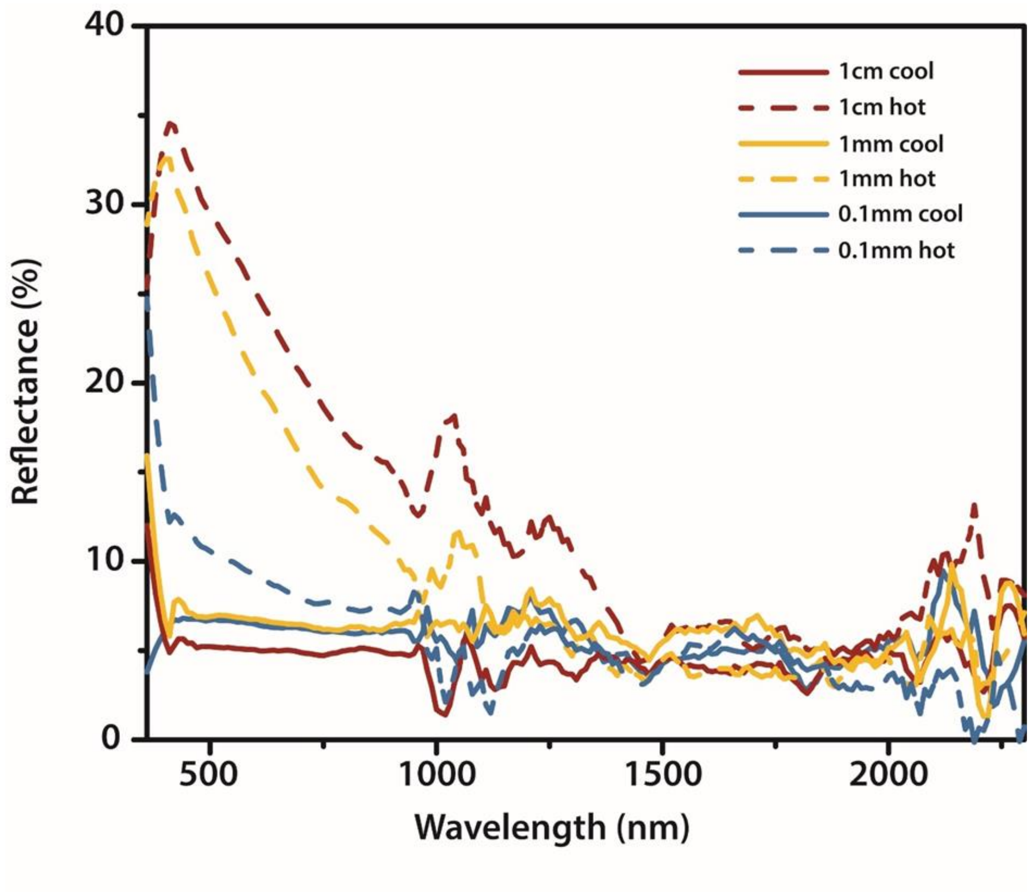

Figure S3. Reflectance spectra for 0.1 mm, 1 mm and 1 cm TRL at 20 °C (solid line) and 60 °C (dashed line), respectively.

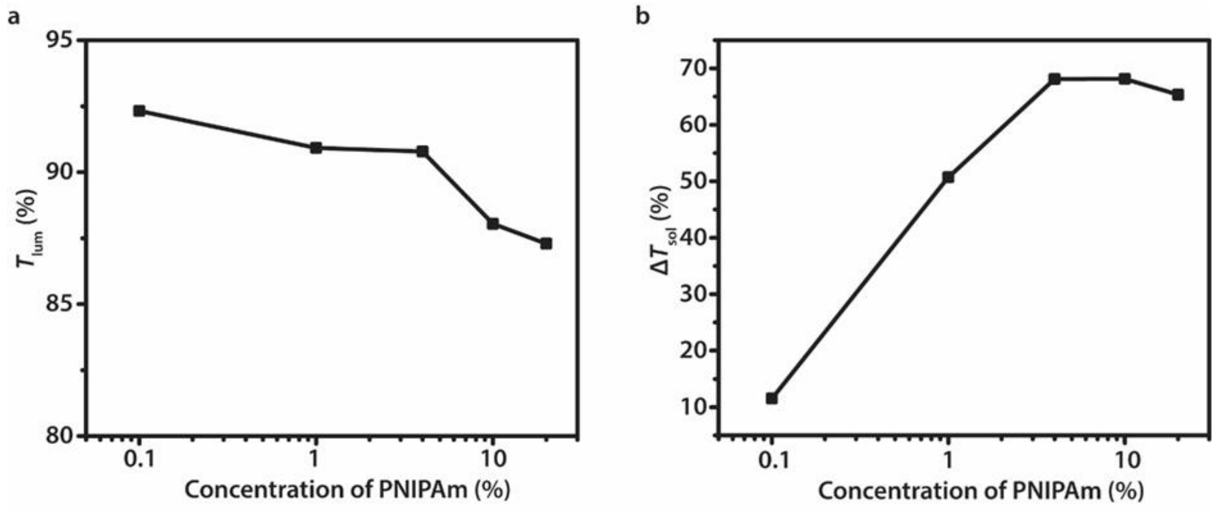

Figure S4. (a) Change of T_{lum} regards to the concentration of PNIPAm changing from 0.1% to 20%. (b) Change of ΔT_{sol} regards to the concentration of PNIPAm changing from 0.1% to 20%.

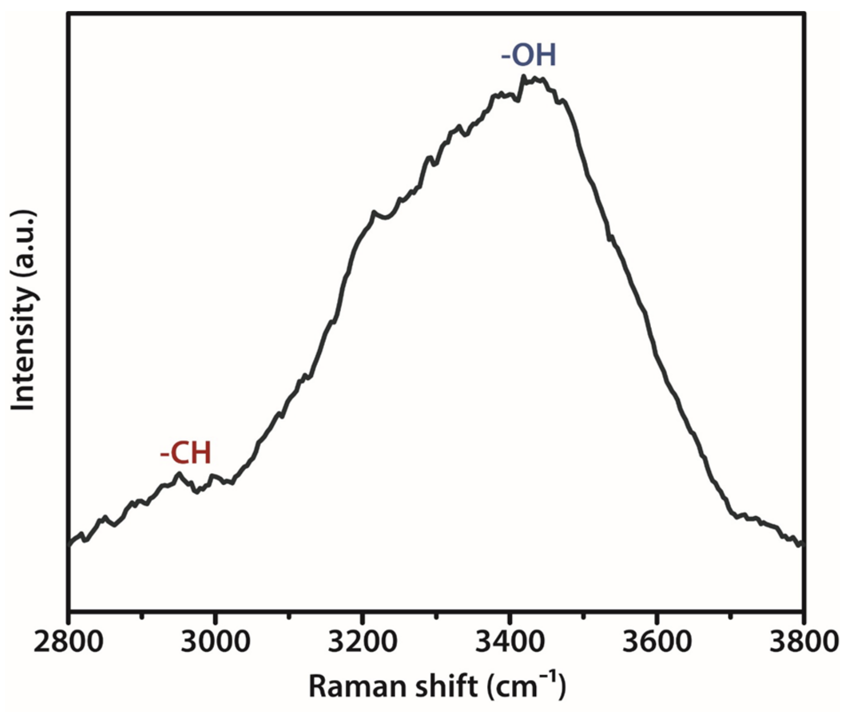

Figure S5. Raman spectrum of PNIPAm

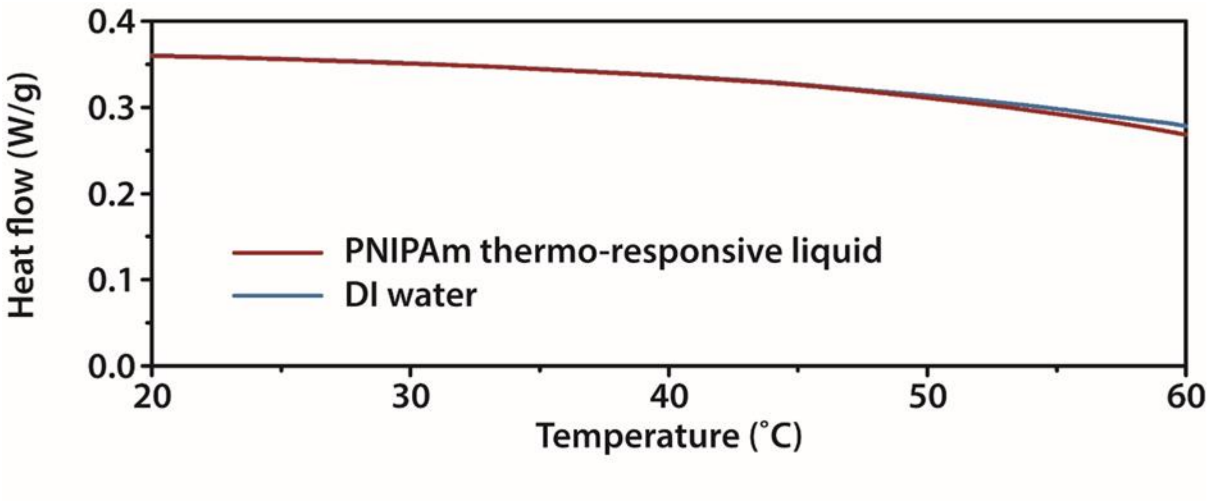

Figure S6. DSC curve for TRL and DI water for the temperature range of 20~60 °C.

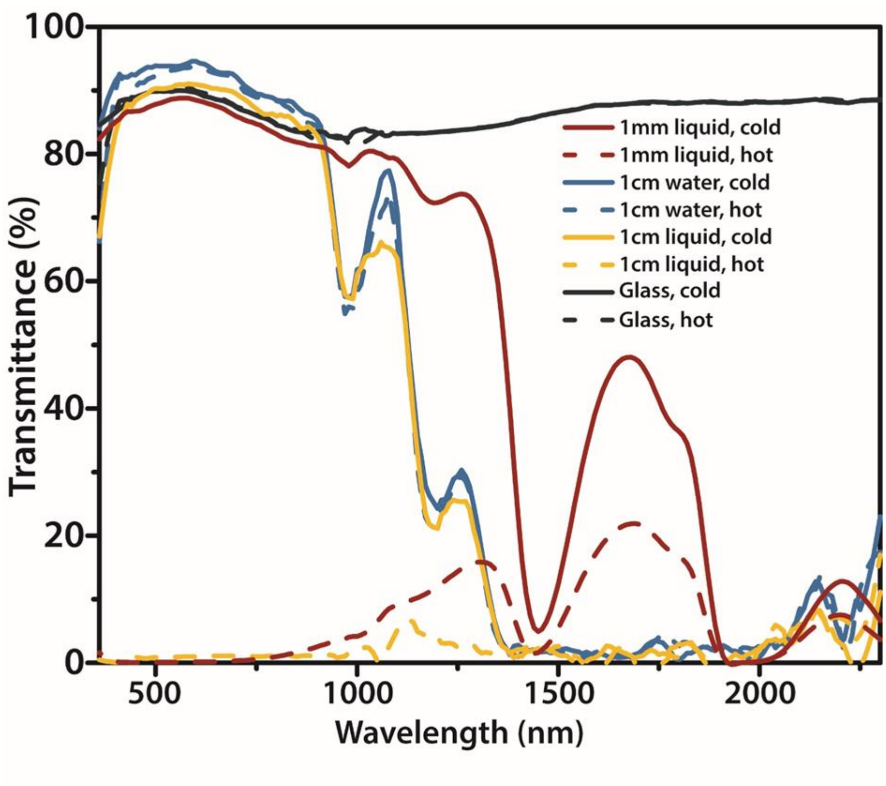

Figure S7. Transmittance spectra for the 1cm thermo-responsive liquid, 1mm high concentration thermo-responsive liquid, 1cm water and normal glass panel at 20°C (cold) and 60°C (hot), respectively.

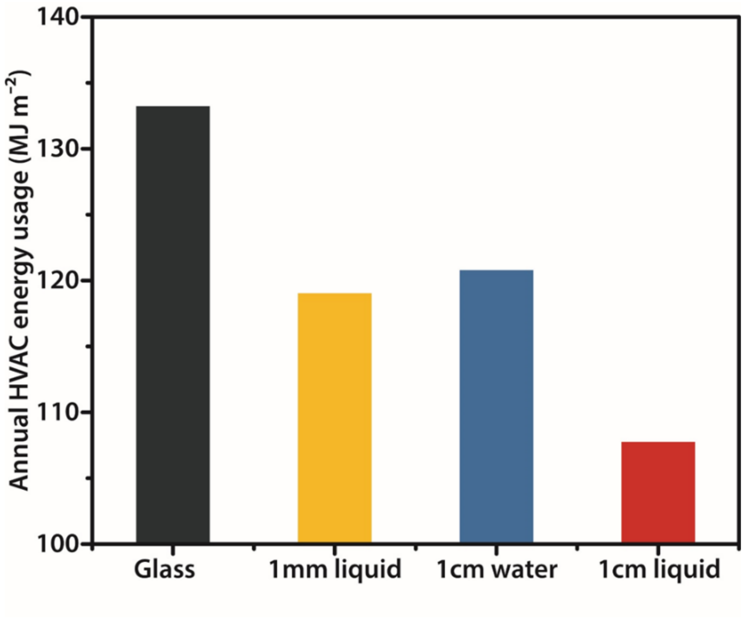

Figure S8. Annual HVAC energy consumption simulation for the glass, 1mm liquid, 1cm water and 1cm liquid, respectively. The climate data in Shanghai is employed in this simulation.

Table S2. Weather condition for the testing date in Singapore, Guangzhou and Beijing, respectively.

City	Date	Sky condition	Highest temperature (°C)	Lowest temperature (°C)
Singapore	17-Feb-2020	Clear	34	26
Guangzhou	04-Nov-2019	Clear	29	18
Beijing	28-Dec-2019	Clear	3	-6

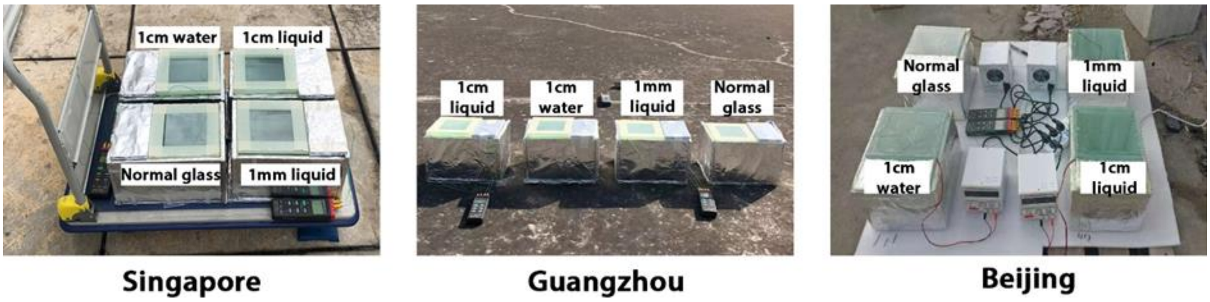

Figure S9. Photo of outdoor test in Singapore, Guangzhou, and Beijing. 1cm liquid filled window, 1cm water filled window, 1mm liquid filled window and the normal glass window were installed on the testing box, respectively. For the test in Beijing, all four boxes were heated up by 10W heater located at the centre of the box.

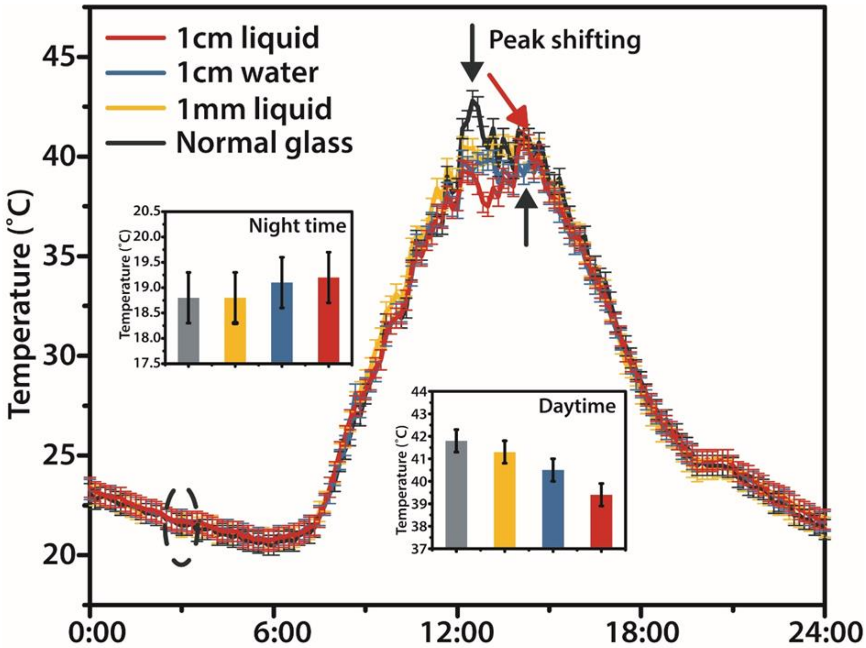

Figure S10. 24 hours air temperature curve for the outdoor demonstration in Guangzhou. The inserts are the daytime (12:00) and night (3:00) temperature reading for normal glass, 1mm liquid, 1cm water and 1cm liquid, respectively. The black arrows indicate the maximum temperature peak for the normal glass and the 1cm liquid, respectively. The error bar for the temperature reading is ±0.5 °C.

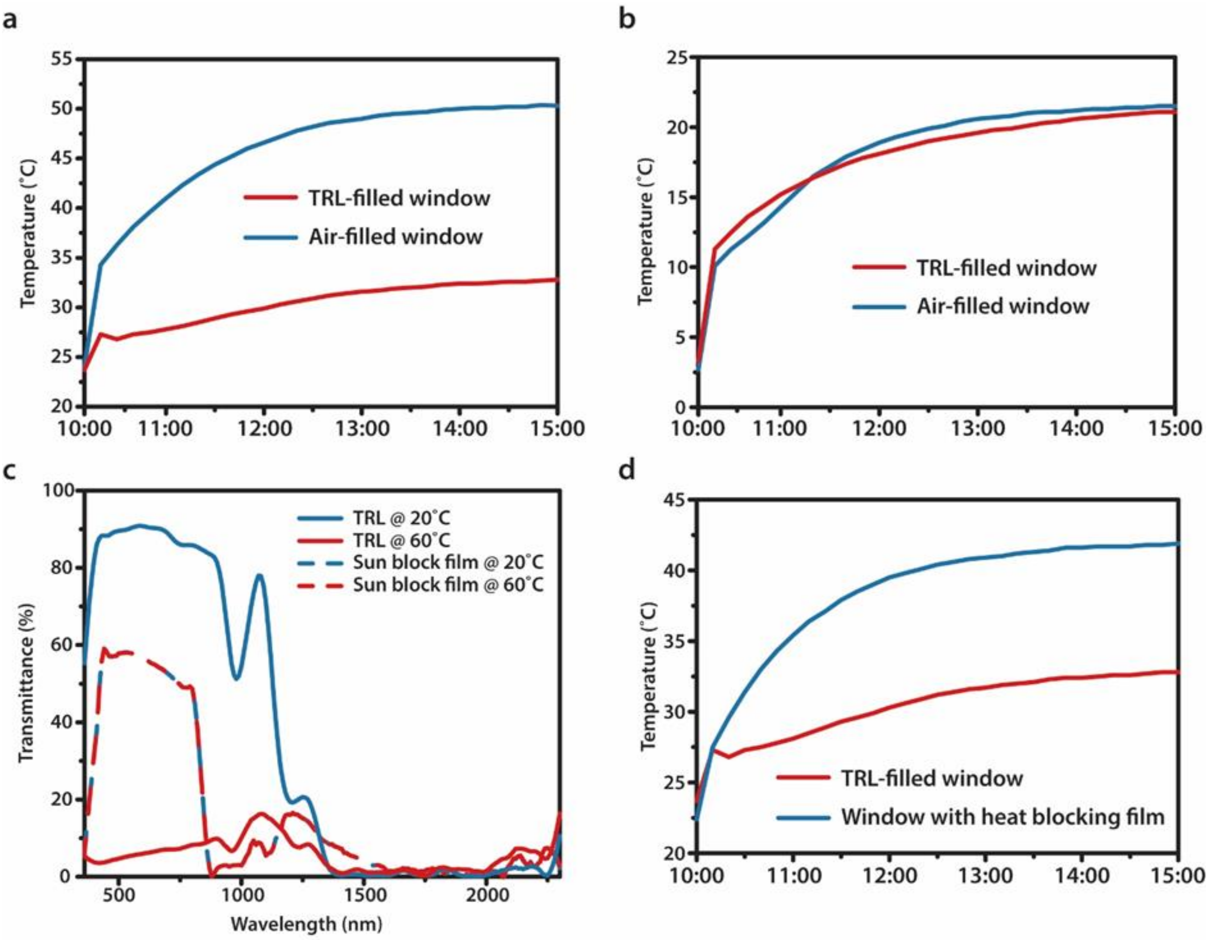

Figure S11. (a) Air temperature for the TRL-filled window and air-filled window in hot environment performance testing. The ambient temperature for the testing was 24 °C. (b) Air temperature for the TRL-filled window and air-filled window in cold environment performance testing. The ambient temperature for the testing was 2 °C. Two 10 W heaters were employed in the testing to serve as the heat source. (c)UV-Vis-NIR spectrum of the 3M™ Prestige70 series heat blocking window film and 1 cm TRL at 20 and 60 °C, respectively. (d) Air temperature for the TRL-filled window and heat blocking film attached window in hot environment performance testing. The ambient temperature for the testing was 24 °C.

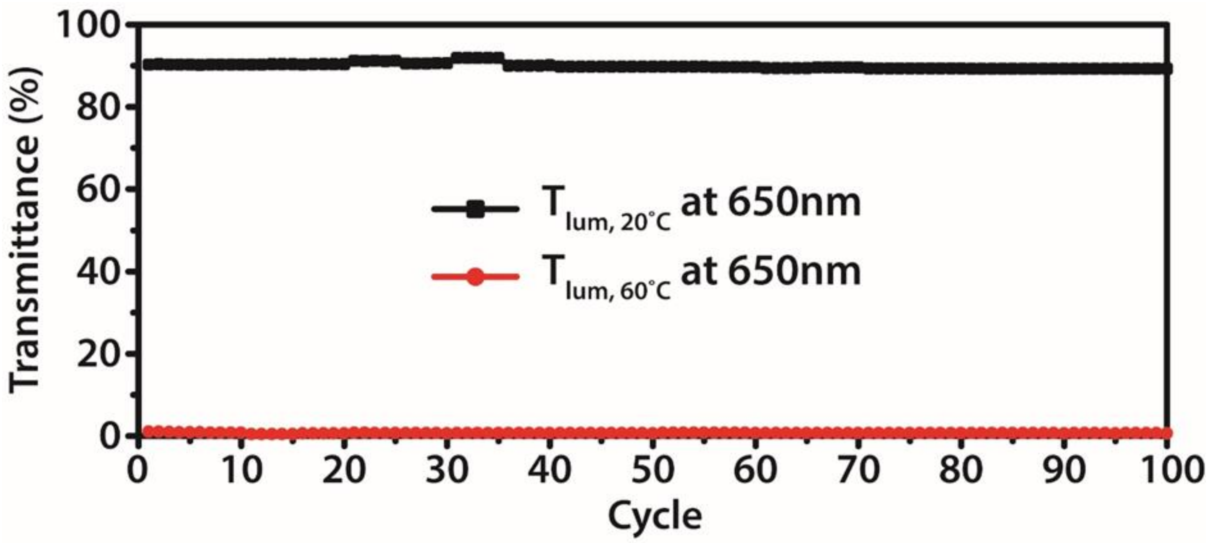

Figure S12. Cycling testing for the HTEST window.

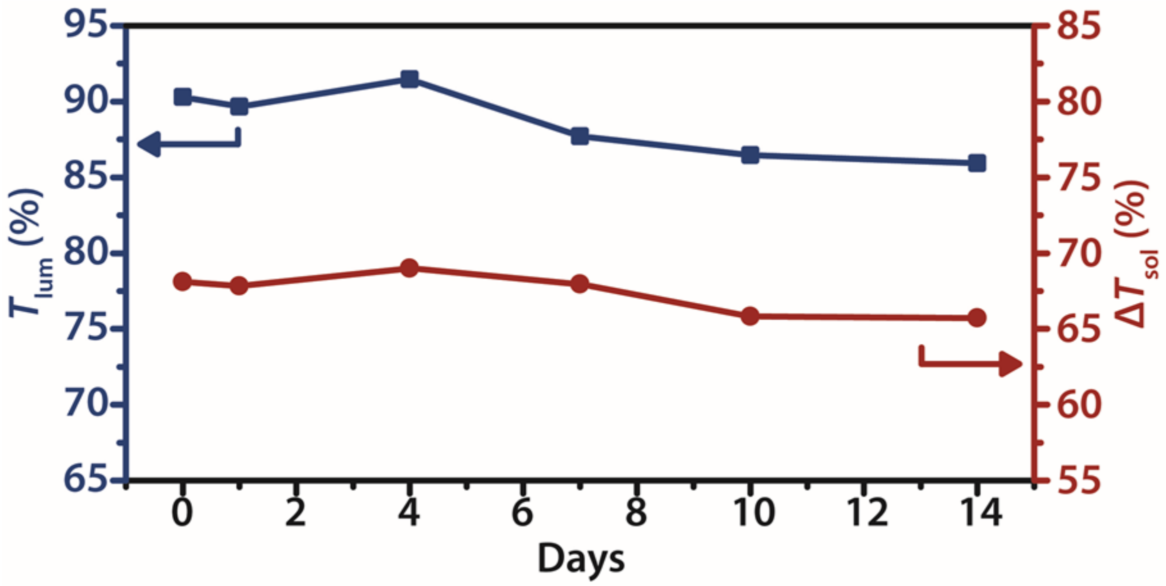

Figure S13. T_{lum} (blue line) and ΔT_{sol} (red line) of TRL versus aging time.

Figure S14. Photo of the 1 m^2 liquid sample for the soundproof testing

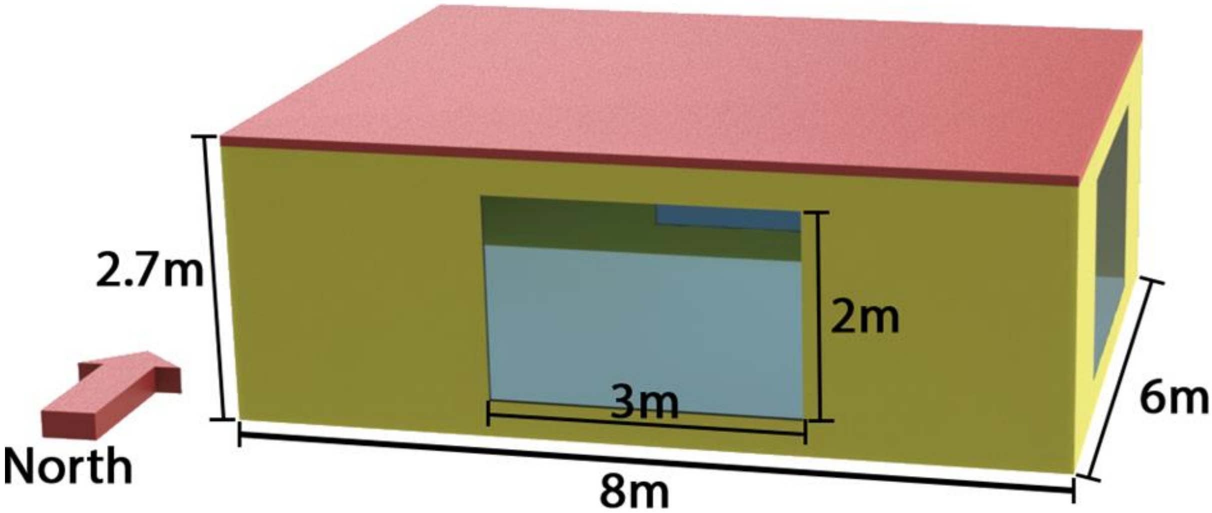

Figure S15. Schematic diagram of the building model used in the simulation

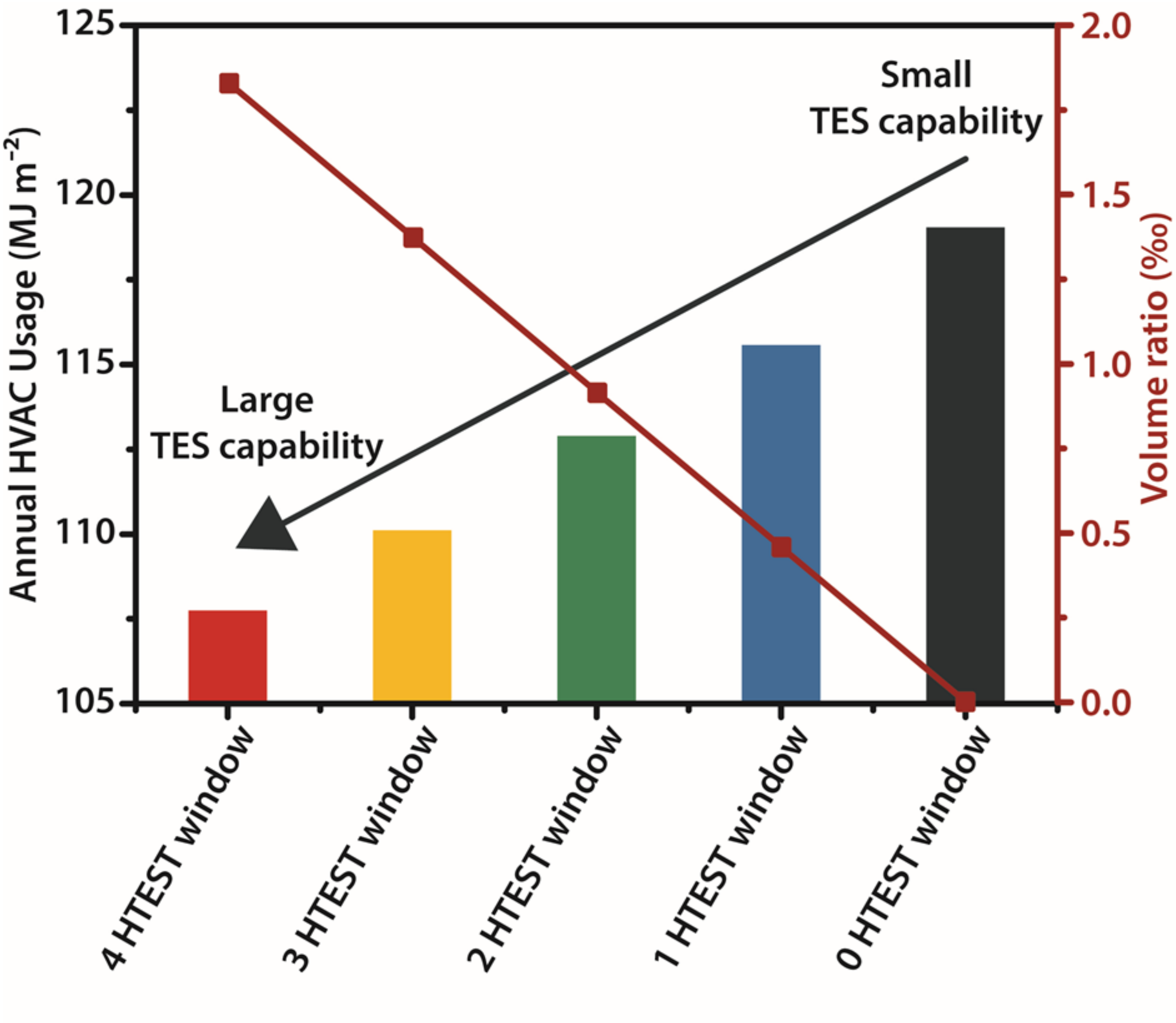

Figure S16. Annual HVAC energy consumption for the house with 4 HTEST window installed, 3 HTEST window and 1 conventional thermochromic window installed, 2 HTEST window and 2 conventional thermochromic window installed, 1 HTEST window and 3 conventional thermochromic window installed and 4 conventional thermochromic window installed, respectively. The line curve and the axis on the right side represents the volume ratio between the TES window and the house.

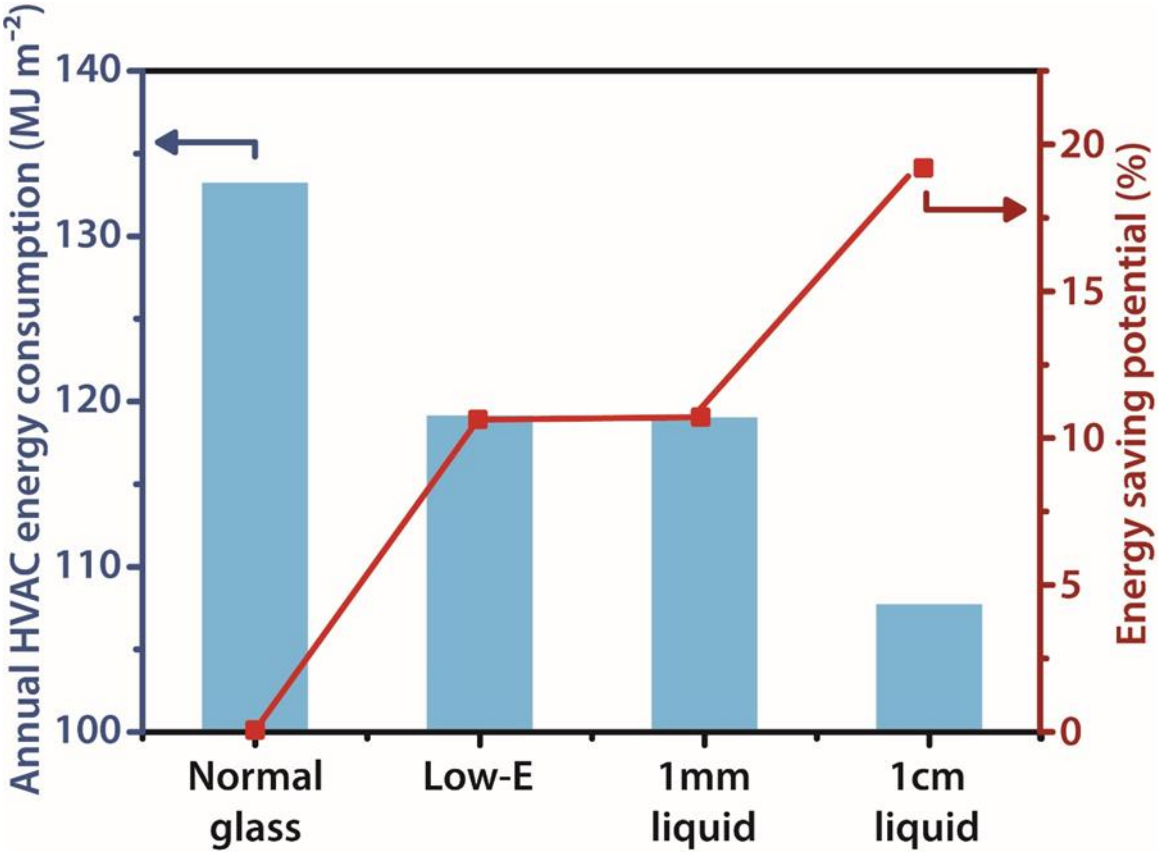

Figure S17. Annual energy saving and energy saving potential simulation in Shanghai.

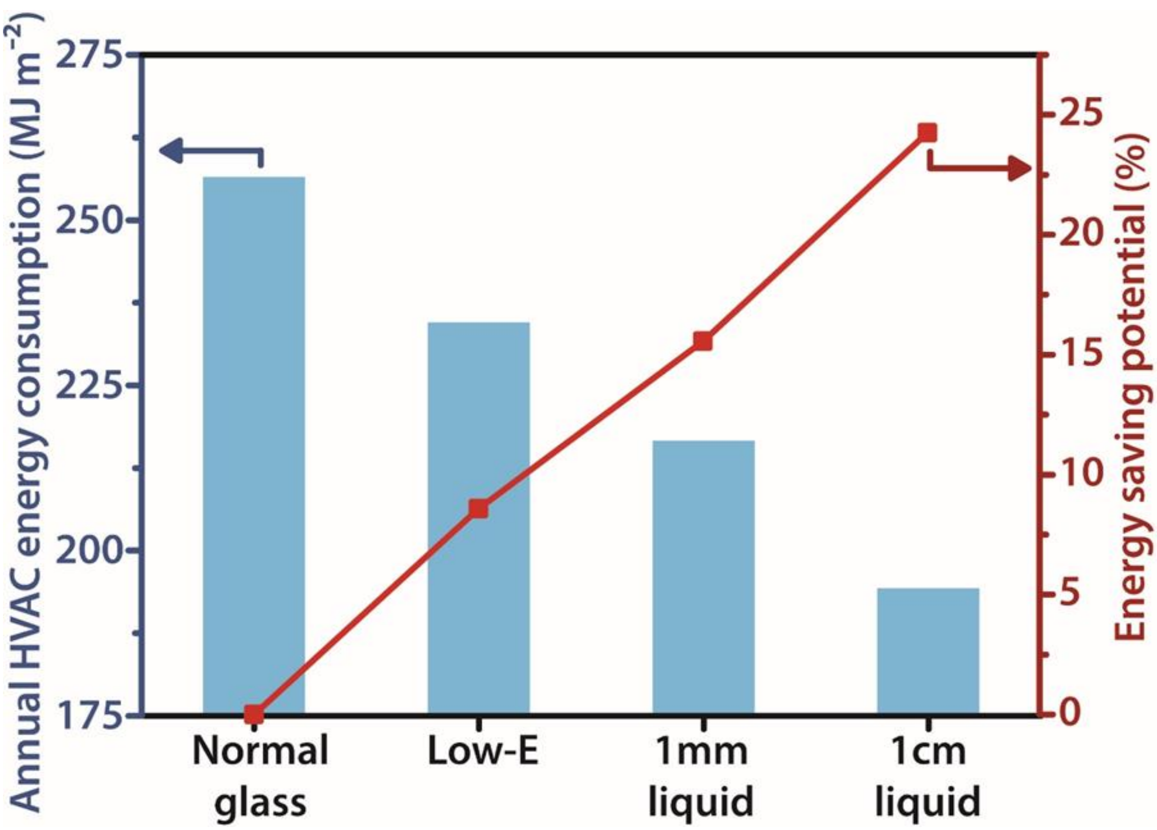

Figure S18. Annual energy saving and energy saving potential simulation in Las Vegas

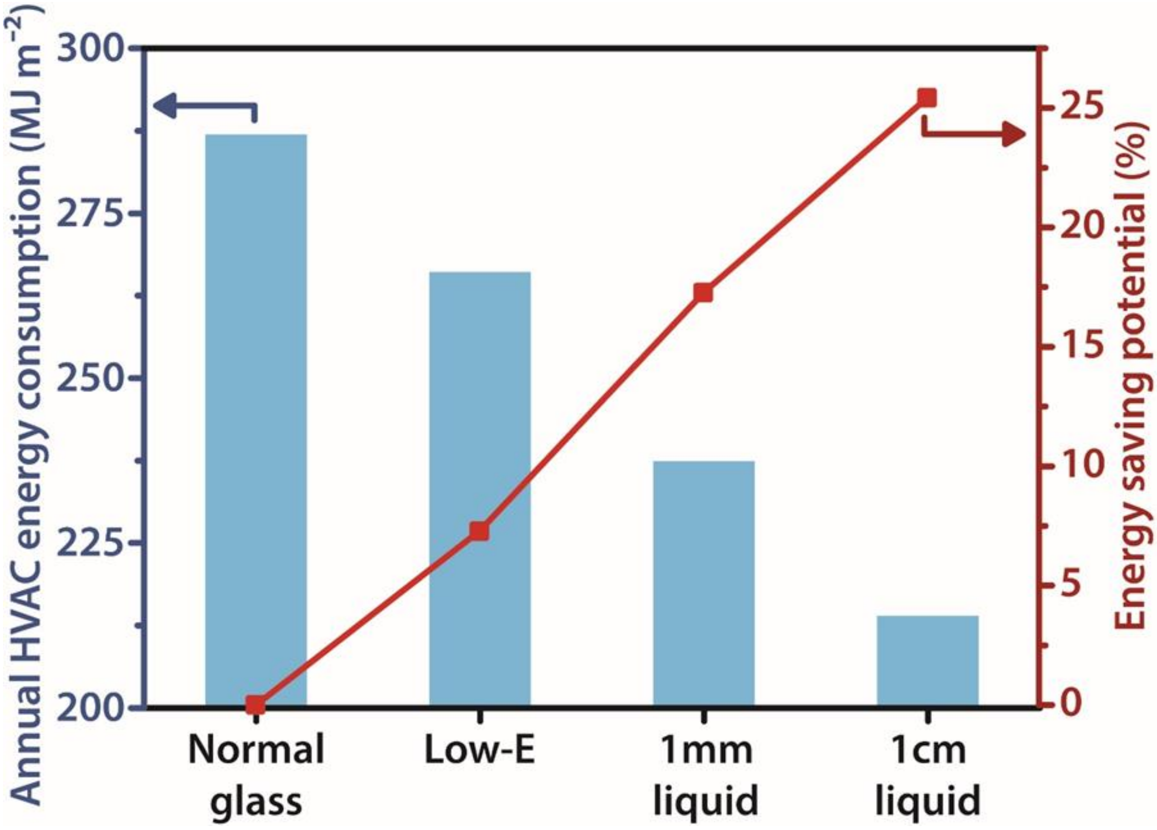

Figure S19. Annual energy saving and energy saving potential simulation in Riyadh

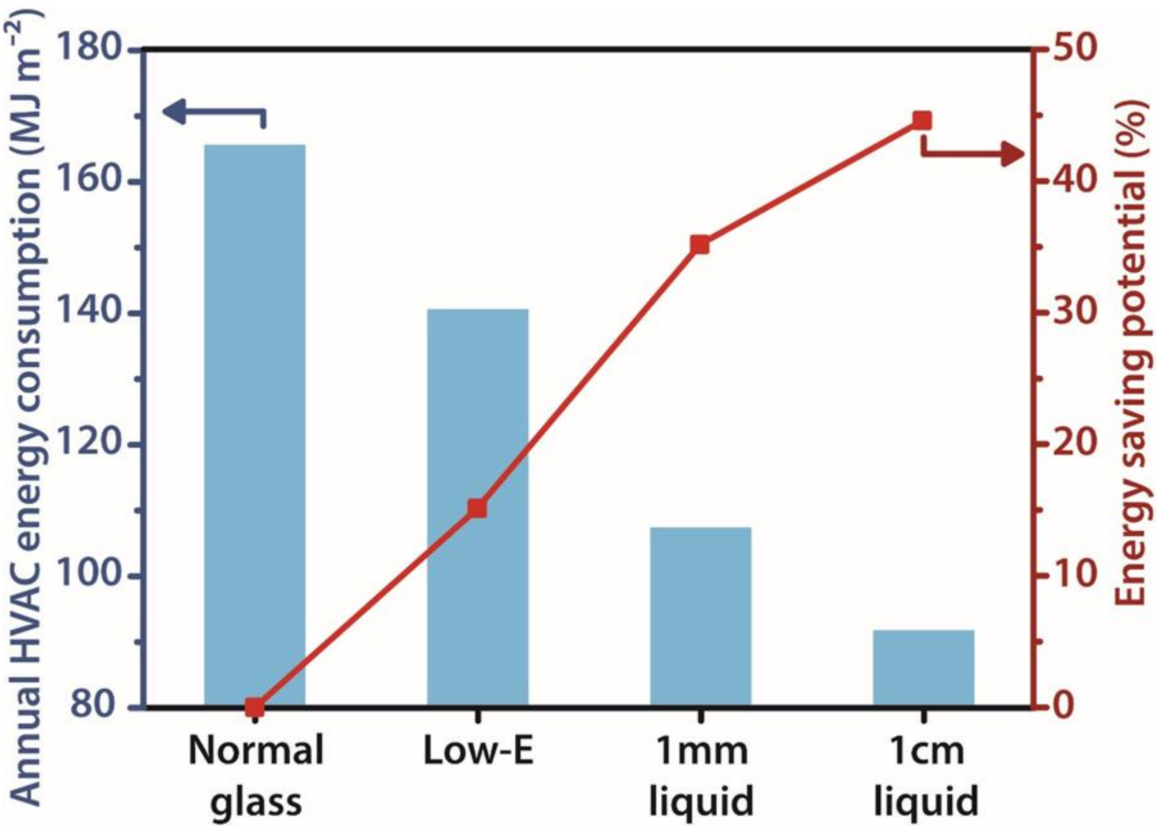

Figure S20. Annual energy saving and energy saving potential simulation in Singapore

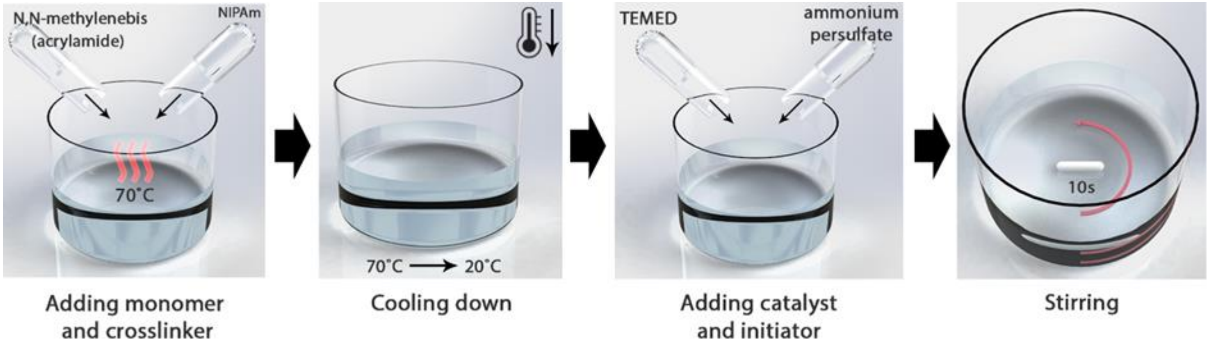

Figure S21. Preparation process of the PNIPAm thermo-responsive liquid

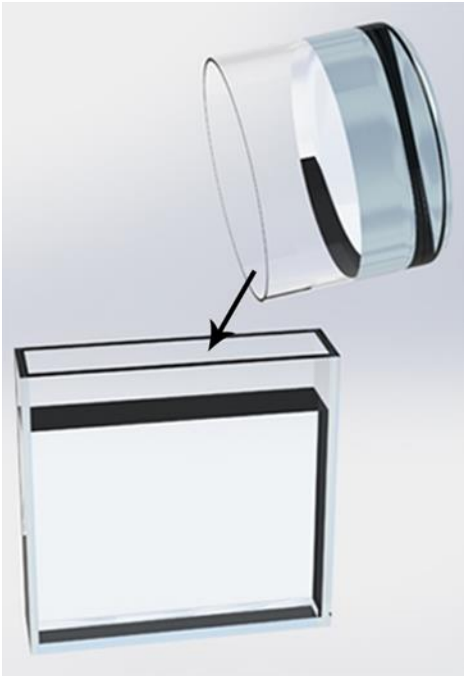

Figure S22. Pouring process of the HTEST smart window

Table S3. Thermal properties of the normal glass window, low-E window, 1mm HTEST window, and 1cm HTEST window

	Normal glass	Low-E	1mm HTEST (20 °C)	1mm HTEST (60 °C)	1cm HTEST (20 °C)	1cm HTEST (60 °C)
U-factor	3.281	2.535	3.284	3.284	3.227	3.227
SHGC	0.677	0.577	0.640	0.368	0.574	0.203